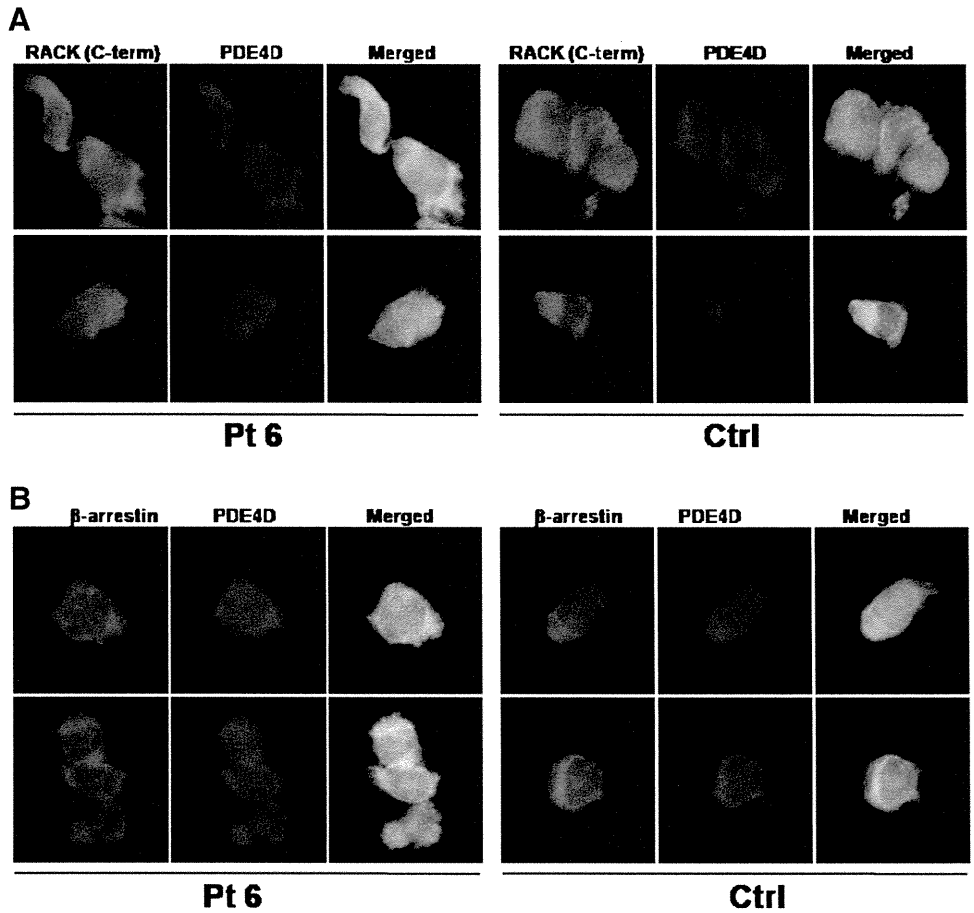

Fig. 5. Intracellular localization of PDE4D, RACK-1, and β-arrestin in EBV-transformed lymphocytes. Panel A shows the localization of PDE4D and RACK-1 in EBV-transformed lymphocytes. Immunofluorescent staining for RACK-1 and PDE4D were performed using rabbit anti-RACK-1 antibody and Alexa488-conjugated goat anti-rabbit IgG (left panel), and goat anti-PDE4D antibody and Alexa568-conjugated donkey anti-goat IgG (middle panel). Nuclei were counterstained with DAPI. Right panels show merged images of RACK-1 and PDE4D. Panel B shows the localization of PDE4D and β-arrestin in EBV-transformed lymphocytes. Immunofluorescent staining for beta-arrestin and PDE4D were performed using mouse anti-β-arrestin antibody and Alexa488-conjugated goat anti-mouse IgG (left panel), and goat anti-PDE4D antibody and Alexa568-conjugated donkey anti-goat IgG (middle panel). Nuclei were counterstained with DAPI. Right panels show merged images of β-arrestin and PDE4D. Colocalization of PDE4D and RACK-1 or β-arrestin was not different in cells from the patient and control subject.

PHP-1a (e.g., AHO) are accompanied by hormonal resistance. Remarkably, hormonal resistance is milder in patients with acrodysostosis caused by the *PRKAR1A* mutation, and even this hormonal resistance is apparently lost in acrodysostosis caused by *PDE4D* mutation. Therefore, hormonal resistance and skeletal dysplasia may represent a spectrum of signal transduction pathway-associated disorders, at least for AHO and acrodysostosis. We suggest that pursuing gene discovery in these diseases should continue, especially in patients who show combined mild hormonal resistance and skeletal manifestations.

In silico 3D structure analyses and in vitro transfection assays, using mutants that reflected those seen in the patients (Figs. 2 and 3), predicted an increase in the cAMP level caused by decreased PDE4D activity. However, our functional analyses of cells from patients with a PDE4D mutation were contradictory to this in that, compared to cells from control subjects, we observed a reduced, rather than an enhanced cAMP accumulation in response to forskolin activation of adenylyl cyclase. However, we resolved the basis of this apparent discrepancy by showing that, in cells from acrodysostosis patients, there appeared to be an up-regulation of PDE4 isoforms from other sub-families whose activity over-compensated for the loss of PDE4D activity (Fig. 4). Thus chronic adaptation to a deficient PDE4D environment appears to foster the over-compensation of the expression of other PDE4 species that likely explains the decreased cAMP accumulation and decreased CREB phosphorylation, compared to cells from normal subjects, seen in cells from acrodysostosis patients in response to forskolin challenge (Figs. 3 and 4). This parallels the situation where PKA activity is compromised by the *PRKAR1A* mutation, as in acrodysostosis without hormone resistance, which may explain why patients with inactivating PDE4D mutations phenotypically show acrodysostosis. Thus, it seems that acrodysostosis patients who are chronically expressing catalytically compromised PDE4D from conception elicits an adaptive response that takes the form of up-regulation of isoforms from other PDE4 subfamilies and that this overcompensates for the reduced activity caused by PDE4D mutation.

The myriad of 20 + PDE4 isoforms are believed to each have distinct, complex promoters but little, however, is known about their precise structure and regulation [65]. Nevertheless, previous studies on PDE4D5, PDE4A11, PDE4D1/2 has shown that they can confer both up- and down-regulation in response to altered cAMP levels [30–33, 66]. Thus analyses of the basis for the up-regulation of PDE4C, PDE4D5 and PDE4D11, which we observed in cells from acrodysostosis patients will require very considerable effort to resolve in future studies. Interestingly, however, there is a paucity of research that has been carried out on the PDE4C gene family and little is known about its precise functional significance, range of isoforms, regulation and distribution, except that it is poorly expressed in the brain [67,68]. However, we now know that an important consequence of PDE4 isoform diversity is that it allows the targeting of particular isoforms to specific signaling complexes,

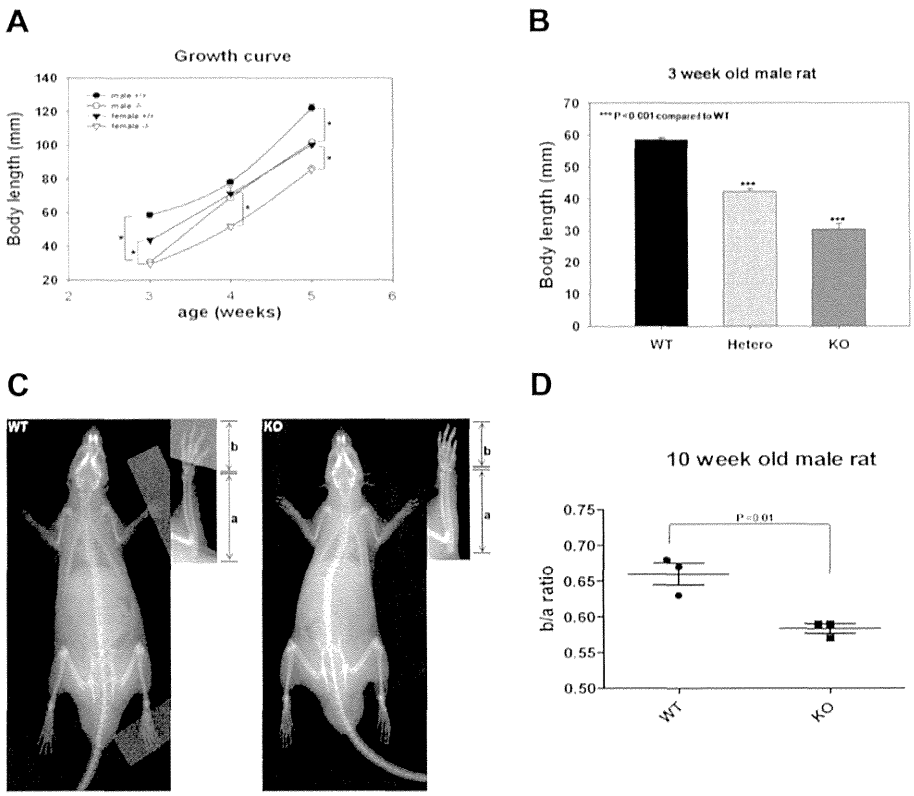

Fig. 6. Skeletal characteristics of PDE4D-KO rats. After birth, WT, heterozygous, and homozygous PDE4D-null rats were examined by measuring body length (nose-to-anus distance, N–A) using digital calipers. A. Starting from postnatal week 3, KO rats appeared significantly smaller than their control littermates. B. Male KO rats were significantly shorter than their WT and heterozygote littermates at 3 weeks. Data are shown as means ± SEM. C and D. The b/a ratios of male KO rats were significantly lower than those of WT rats at 10 weeks. Decreased b/a ratios correspond to brachydactyly, which is seen in patients with acrodysostosis. (a: length of a forearm; b: length of a forepaw).

which allows them to exert distinct functional roles [18]. Thus, while up-regulation of PDE4C may compensate for a lowering of overall PDE4 activity due to chronic expression of the mutant PDE4D isoforms, PDE4C is unlikely to result in identical sequestration of the same signaling complexes in cells that would be seen with the various PDE4D isoforms. This 'failure' is likely to elicit an up-regulation of PDE4C to higher levels than to be seen with PDE4D, as the cell strives to generate enough active PDE4 to pair with the signaling complexes involving PDE4D. Additionally, the mass action effect due to the increased level of PDE4 isoform expression in acrodysostosis with hormone resistance patients is likely to cause increased sequestration of binding partners involving PDE4C and PDE4D5/11, which may itself lead to functional changes [7].

The patients with *PDE4D* mutations notably had no apparent hormone resistance, unlike the patients with *PRKAR1A* mutations [5]. Our patient 3, who harbored the *PRKAR1A* mutation, as well as three patients with the same mutation in the previous report, had hormone resistance. However, our patients with *PDE4D* mutations did not show any clinical evidence of hormone resistance. One possible explanation for the presence or absence of hormone resistance in *PDE4D*-related acrodysostosis is related to the extreme diversity of the PDE isoenzymes and their tissue-specific patterns of expression. In fact, PDE4 is one of the main isoenzymes in the osteoblast [69]. On the other hand, *PRKAR1A* is a common pathway gene in the Gsα-cAMP-PKA signal transduction pathway; therefore, mutation in this gene may cause acrodysostosis as well as hormone resistance [70]. Another possibility is that if the core acrodysostosis phenotype in *PDE4D* mutation patients is due to compensatory up-regulation of PDE4C, with concomitant down-regulation of PKA activity and CREB phosphorylation, then the lack of hormone resistance may be due to the lowered PDE4D activity. This can be expected to allow activation of a pool of PKA sequestered close to it, as we have shown in 'dominant negative' approaches [21]. This would allow a key difference with *PRKAR1A* mutations, where all of the PKA-RI activity is compromised, to the *PDE4D* mutations where we propose that the major pool of PKA-RI activity will be compromised due to PDE4C up-regulation, while a PKA-RI pool associated with catalytically compromised PDE4D will be more active. Possibly, phosphorylation of a hormone receptor component associated with a PKA/PDE4D signaling complex negates hormone resistance in patients *PDE4D* mutations.

Finally, we tried to prove that loss of function of PDE4D in the long run results in the abnormalities of skeletal bone formation, as in human. In order to undertake this we employed a PDE4D knockout analysis using the rat, as mice are too small to discern the level of phenotypic change of KO expected. To address this hypothesis, we generated, for the first time, a KO of PDE4D in the rat; a larger rodent. In humans, skeletal manifestation of acrodysostosis without hormonal resistance consists of short stature, shortening of the distal part of the limb (especially the metacarpals and phalanges), and nasal bone hypoplasia. Nasal bone changes in the KO rat were difficult to discern. However, other manifestations in the bones were evident including significantly stunted growth in each gender at the age of 3 and 5 weeks. Moreover, this stunted growth was observed both in the KO rat and in heterozygote rats, as was it indeed noted in PDE4D deficient mice [71]. The most intriguing finding in this model was the observation that skeletal radiographs of 10-week-old KO rats showed shorter distal parts of the forelimbs (radius and palm) than in wild type rats and all of the metacarpals and phalanges of KO rat were also shorter than in the WT rat, as the name acrodysostosis implies. Our results show the strength of the KO rat model in terms of observing the relative bone change in the small bones.

It remains to be appreciated as to which specific PDE4D isoforms are critical to this pathology and whether mutations affect distinct isoform

differently. Certainly there is a growing appreciation that PDE4D isoforms perform distinct functional roles (see e.g. [21] and can provide important regulatory enzymes that affect cell proliferation [72]) and the cell cycle [73].

5. Conclusions

In conclusion, as has been observed with GNAS and PRKAR1A, PDE4D serves as a key regulatory element in the cAMP signal transduction pathway and influences bone formation that leads to skeletal dysplasia. We propose that specific inhibitory PDE4D mutations provide the focus that triggers the molecular pathology of acrodysostosis without hormone resistance. However, we need to appreciate that aspects of the pathological phenotype may well also be dependent on an over-compensatory induction of other PDE4 isoforms that can be expected to be targeted to different signaling complexes and exert distinct effects on compartmentalized cAMP signaling.

Conflict of interest

All of the authors have no conflict of interest.

Acknowledgments

This study was supported by grants from the Korea Healthcare Technology R&D Project, Ministry for Health, Welfare and Family Affairs, Republic of Korea (A080588), the Samsung Biomedical Research Institute grant (SBRI C-A9-240-3), the Korea Science and Engineering Foundation (KOSEF) grant funded by the Korean government (MEST) (no. 2008-006198), Center for Clinical Research (PHO 1100931 Green Cross), and a grant from the Ministry of Health, Labour and Welfare, Japan (H23-Jitsuyoka(Nanbyo)-Ippan-007). We thank KIAS Center for Advanced Computation for providing the Linux cluster system for computational modeling.

References

[1] L.C. Wilson, M.E. Oude Luttikhuis, M. Baraitser, H.M. Kingston, R.C. Trembath, J. Med. Genet. 34 (1997) 133–136.
[2] M.G. Butler, L.J. Rames, W.B. Wadlington, Am. J. Med. Genet. 30 (1988) 971–980.
[3] M.D. Houslay, G. Milligan, Trends Biochem. Sci. 22 (1997) 217–224.
[4] J.M. Graham Jr., D. Krakow, V.T. Tolo, A.K. Smith, R.S. Lachman, Pediatr. Radiol. 31 (2001) 2–9.
[5] A. Linglart, C. Menguy, A. Couvineau, C. Auzan, Y. Gunes, M. Cancel, E. Motte, G. Pinto, P. Chanson, P. Bougneres, E. Clauser, C. Silve, N. Engl. J. Med. 364 (2011) 2218–2226.
[6] M. Breckler, M. Berthouze, A.C. Laurent, B. Crozatier, E. Morel, F. Lezoualc'h, Cell. Signal. 23 (2011) 1257–1266.
[7] M.D. Houslay, Trends Biochem. Sci. 35 (2010) 91–100.
[8] C. Lugnier, Pharmacol. Ther. 109 (2006) 366–398.
[9] M.D. Houslay, P. Schafer, K.Y. Zhang, Drug Discov. Today 10 (2005) 1503–1519.
[10] C.P. Page, D. Spina, Curr. Opin. Pharmacol. 12 (2012) 275–286.
[11] C.P. Page, D. Spina, Handb. Exp. Pharmacol. (2011) 391–414.
[12] B. Beghe, K.F. Rabe, L.M. Fabbri, Am. J. Respir. Crit. Care Med. 188 (2013) 271–278.
[13] A. Hatzelmann, E.J. Morcillo, G. Lungarella, S. Adnot, S. Sanjar, R. Beume, C. Schudt, H. Tenor, Pulm. Pharmacol. Ther. 23 (2010) 235–256.
[14] K.F. Rabe, Br. J. Pharmacol. 163 (2011) 53–67.
[15] P.H. Schafer, R.M. Day, J. Am. Acad. Dermatol. 68 (2013) 1041–1042.
[16] M. Wittmann, P.S. Helliwell, Dermatol. Ther. (Heidelb) 3 (2013) 1–15.
[17] M. Conti, J. Beavo, Annu. Rev. Biochem. 76 (2007) 481–511.
[18] T. Keravis, C. Lugnier, Curr. Pharm. Des. 16 (2010) 1114–1125.
[19] M.D. Houslay, G.S. Baillie, D.H. Maurice, Circ. Res. 100 (2007) 950–966.
[20] K. McCormick, G.S. Baillie, Curr. Opin. Genet. Dev. 27C (2014) 20–25.
[21] A. McCahill, T. McSorley, E. Huston, E.V. Hill, M.J. Lynch, I. Gall, G. Keryer, B. Lygren, K. Tasken, G. van Heeke, M.D. Houslay, Cell. Signal. 17 (2005) 1158–1173.
[22] G.B. Bolger, G.S. Baillie, X. Li, M.J. Lynch, P. Herzyk, A. Mohamed, L.H. Mitchell, A. McCahill, C. Hundsrucker, E. Klussmann, D.R. Adams, M.D. Houslay, Biochem. J. 398 (2006) 23–36.
[23] G.S. Baillie, A. Sood, I. McPhee, I. Gall, S.J. Perry, R.J. Lefkowitz, M.D. Houslay, Proc. Natl. Acad. Sci. U. S. A. 100 (2003) 940–945.
[24] A. Terrin, S. Monterisi, A. Stangherlin, A. Zoccarato, A. Koschinski, N.C. Surdo, M. Mongillo, A. Sawa, N.E. Jordanides, J.C. Mountford, M. Zaccolo, J. Cell Biol. 198 (2012) 607–621.
[25] M.J. Lynch, G.S. Baillie, A. Mohamed, X. Li, C. Maisonneuve, E. Klussmann, G. van Heeke, M.D. Houslay, J. Biol. Chem. 280 (2005) 33178–33189.
[26] Y. Shakur, J.G. Pryde, M.D. Houslay, Biochem. J. 292 (Pt 3) (1993) 677–686.
[27] E. Huston, I. Gall, T.M. Houslay, M.D. Houslay, J. Cell Sci. 119 (2006) 3799–3810.
[28] G.S. Baillie, E. Huston, G. Scotland, M. Hodgkin, I. Gall, A.H. Peden, C. MacKenzie, E.S. Houslay, R. Currie, T.R. Pettitt, A.R. Walmsley, M.J. Wakelam, J. Warwicker, M.D. Houslay, J. Biol. Chem. 277 (2002) 28298–28309.
[29] M.J. Lynch, G.S. Baillie, M.D. Houslay, Biochem. Soc. Trans. 35 (2007) 938–941.
[30] E. Vicini, M. Conti, Mol. Endocrinol. 11 (1997) 839–850.
[31] I.R. Le Jeune, M. Shepherd, G. Van Heeke, M.D. Houslay, I.P. Hall, J. Biol. Chem. 277 (2002) 35980–35989.
[32] D.A. Wallace, L.A. Johnston, E. Huston, D. MacMaster, T.M. Houslay, Y.F. Cheung, L. Campbell, J.E. Millen, R.A. Smith, I. Gall, R.G. Knowles, M. Sullivan, M.D. Houslay, Mol. Pharmacol. 67 (2005) 1920–1934.
[33] A. McCahill, L. Campbell, T. McSorley, A. Sood, M.J. Lynch, X. Li, C. Yan, G.S. Baillie, M.D. Houslay, (PDE4A10), Cell. Signal. 20 (2008) 2071–2083.
[34] G. Bolger, T. Michaeli, T. Martins, T. St John, B. Steiner, L. Rodgers, M. Riggs, M. Wigler, K. Ferguson, Mol. Cell. Biol. 13 (1993) 6558–6571.
[35] C. Sette, M. Conti, J. Biol. Chem. 271 (1996) 16526–16534.
[36] N. Oki, S.I. Takahashi, H. Hidaka, M. Conti, J. Biol. Chem. 275 (2000) 10831–10837.
[37] D. Mika, W. Richter, R.E. Westenbroek, W.A. Catterall, M. Conti, J. Cell Sci. 127 (2014) 1033–1042.
[38] D. Willoughby, G.S. Baillie, M.J. Lynch, A. Ciruela, M.D. Houslay, D.M. Cooper, J. Biol. Chem. 282 (2007) 34235–34249.
[39] R. Hoffmann, I.R. Wilkinson, J.F. McCallum, P. Engels, M.D. Houslay, Biochem. J. 333 (Pt 1) (1998) 139–149.
[40] M.B. Beard, A.E. Olsen, R.E. Jones, S. Erdogan, M.D. Houslay, G.B. Bolger, J. Biol. Chem. 275 (2000) 10349–10358.
[41] S.J. MacKenzie, G.S. Baillie, I. McPhee, C. MacKenzie, R. Seamons, T. McSorley, J. Millen, M.B. Beard, G. van Heeke, M.D. Houslay, (UCR1), Br. J. Pharmacol. 136 (2002) 421–433.
[42] D.M. Collins, H. Murdoch, A.J. Dunlop, E. Charych, G.S. Baillie, Q. Wang, F.W. Herberg, N. Brandon, A. Prinz, M.D. Houslay, (PDE4D3) in a manner that is dynamically regulated through Protein Kinase A (PKA), Cell. Signal. 20 (2008) 2356–2369.
[43] K.F. MacKenzie, D.A. Wallace, E.V. Hill, D.F. Anthony, D.J. Henderson, D.M. Houslay, J. S. Arthur, G.S. Baillie, M.D. Houslay, Biochem. J. 435 (2011) 755–769.
[44] N. Niikawa, I. Matsuda, T. Ohsawa, T. Kajii, Hum. Genet. 42 (1978) 227–232.
[45] J.M. Ko, K.S. Kwack, S.-H. Kim, H.-J. Kim, J. Genet. Med. 7 (2010) 145–150.
[46] E. Nii, M. Urawa, T. Nshimura, H. Kitou, S. Ikegawa, S. Shimizu, H. Taneda, A. Uchida, N. Niikawa, Am. J. Med. Genet. B Neuropsychiatr. Genet. 144B (2007) 824–825.
[47] G.B. Bolger, S. Erdogan, R.E. Jones, K. Loughney, G. Scotland, R. Hoffmann, I. Wilkinson, C. Farrell, M.D. Houslay, Biochem. J. 328 (Pt 2) (1997) 539–548.
[48] K. Joo, J. Lee, S. Lee, J.H. Seo, S.J. Lee, J. Lee, Proteins 69 (Suppl. 8) (2007) 83–89.
[49] K. Joo, J. Lee, I. Kim, S.J. Lee, J. Lee, Biophys. J. 95 (2008) 4813–4819.
[50] K. Joo, J. Lee, J.H. Seo, K. Lee, B.G. Kim, J. Lee, Proteins 75 (2009) 1010–1023.
[51] M. Tress, J. Cheng, P. Baldi, K. Joo, J. Lee, J.H. Seo, J. Lee, D. Baker, D. Chivian, D. Kim, I. Ezkurdia, Proteins 69 (Suppl. 8) (2007) 137–151.
[52] O. Trott, A.J. Olson, J. Comput. Chem. 31 (2010) 455–461.
[53] B. Lu, A.M. Geurts, C. Poirier, D.C. Petit, W. Harrison, P.A. Overbeek, C.E. Bishop, Mamm. Genome 18 (2007) 338–346.
[54] G.S. Baillie, FEBS J. 276 (2009) 1790–1799.
[55] M.D. Houslay, D.R. Adams, Biochem. J. 370 (2003) 1–18.
[56] K.J. Smith, G.S. Baillie, E.I. Hyde, X. Li, T.M. Houslay, A. McCahill, A.J. Dunlop, G.B. Bolger, E. Klussmann, D.R. Adams, M.D. Houslay, Cell. Signal. 19 (2007) 2612–2624.
[57] H.V. Edwards, F. Christian, G.S. Baillie, Semin. Cell Dev. Biol. 23 (2012) 181–190.
[58] B.E. Himes, G.M. Hunninghake, J.W. Baurley, N.M. Rafaels, P. Sleiman, D.P. Strachan, J. B. Wilk, S.A. Willis-Owen, B. Klanderman, J. Lasky-Su, R. Lazarus, A.J. Murphy, M.E. Soto-Quiros, L. Avila, T. Beaty, R.A. Mathias, I. Ruczinski, K.C. Barnes, J.C. Celedon, W.O. Cookson, W.J. Gauderman, F.D. Gilliland, H. Hakonarson, C. Lange, M.F. Moffatt, G.T. O'Connor, B.A. Raby, E.K. Silverman, S.T. Weiss, Am. J. Hum. Genet. 84 (2009) 581–593.
[59] S. Shifman, A. Bhomra, S. Smiley, N.R. Wray, M.R. James, N.G. Martin, J.M. Hettema, S.S. An, M.C. Neale, E.J. van den Oord, K.S. Kendler, X. Chen, D.I. Boomsma, C.M. Middeldorp, J.J. Hottenga, P.E. Slagboom, J. Flint, Mol. Psychiatry 13 (2008) 302–312.
[60] S. Gretarsdottir, G. Thorleifsson, S.T. Reynisdottir, A. Manolescu, S. Jonsdottir, T. Jonsdottir, T. Gudmundsdottir, S.M. Bjarnadottir, O.B. Einarsson, H.M. Gudjonsdottir, M. Hawkins, G. Gudmundsson, H. Gudmundsdottir, H. Andrason, A.S. Gudmundsdottir, M. Sigurdardottir, T.T. Chou, J. Nahmias, S. Goss, S. Sveinbjornsdottir, E.M. Valdimarsson, F. Jakobsson, U. Agnarsson, V. Gudnason, G. Thorgeirsson, J. Fingerle, M. Gurney, D. Gudbjartsson, M.L. Frigge, A. Kong, K. Stefansson, J.R. Gulcher, Nat. Genet. 35 (2003) 131–138.
[61] C. Wu, Z. Hu, Z. He, W. Jia, F. Wang, Y. Zhou, Z. Liu, Q. Zhan, Y. Liu, D. Yu, K. Zhai, J. Chang, Y. Qiao, G. Jin, Z. Liu, Y. Shen, C. Guo, J. Fu, X. Miao, W. Tan, H. Shen, Y. Ke, Y. Zeng, T. Wu, D. Lin, Nat. Genet. 43 (2011) 679–684.
[62] C. Michot, C. Le Goff, A. Goldenberg, A. Abhyankar, C. Klein, E. Kinning, A.M. Guerrot, P. Flahaut, A. Duncombe, G. Baujat, S. Lyonnet, C. Thalassinos, P. Nitschke, J.L. Casanova, M. Le Merrer, A. Munnich, V. Cormier-Daire, Am. J. Hum. Genet. 90 (2012) 740–745.
[63] H. Lee, J.M. Graham Jr., D.L. Rimoin, R.S. Lachman, P. Krejci, S.W. Tompson, S.F. Nelson, D. Krakow, D.H. Cohn, Am. J. Hum. Genet. 90 (2012) 746–751.
[64] L.S. Kirschner, J.A. Carney, S.D. Pack, S.E. Taymans, C. Giatzakis, Y.S. Cho, Y.S. Cho-Chung, C.A. Stratakis, Nat. Genet. 26 (2000) 89–92.
[65] M.D. Houslay, Prog. Nucleic Acid Res. Mol. Biol. 69 (2001) 249–315.

[66] G. Rena, F. Begg, A. Ross, C. MacKenzie, I. McPhee, L. Campbell, E. Huston, M. Sullivan, M.D. Houslay, Mol. Pharmacol. 59 (2001) 996–1011.
[67] M. Sullivan, A.S. Olsen, M.D. Houslay, Cell. Signal. 11 (1999) 735–742.
[68] R.J. Owens, S. Lumb, K. Rees-Milton, A. Russell, D. Baldock, V. Lang, T. Crabbe, M. Ballesteros, M.J. Perry, Cell. Signal. 9 (1997) 575–585.
[69] S. Wakabayashi, T. Tsutsumimoto, S. Kawasaki, T. Kinoshita, H. Horiuchi, K. Takaoka, J. Bone Miner. Res. 17 (2002) 249–256.
[70] S.R. Neves, P.T. Ram, R. Iyengar, Science 296 (2002) 1636–1639.
[71] S.L. Jin, F.J. Richard, W.P. Kuo, A.J. D'Ercole, M. Conti, Proc. Natl. Acad. Sci. U. S. A. 96 (1999) 11998–12003.
[72] D.J. Henderson, A. Byrne, K. Dulla, G. Jenster, R. Hoffmann, G.S. Baillie, M.D. Houslay, Br. J. Cancer 110 (2014) 1278–1287.
[73] C.L. Sheppard, L.C. Lee, E.V. Hill, D.J. Henderson, D.F. Anthony, D.M. Houslay, K.C. Yalla, L.S. Cairns, A.J. Dunlop, G.S. Baillie, E. Huston, M.D. Houslay, Cell. Signal. 26 (2014) 1958–1974.

CLINICAL GENETICS An International Journal of Genetics, Molecular and Personalized Medicine

Clin Genet 2014
Printed in Singapore. All rights reserved

Published by John Wiley & Sons Ltd
CLINICAL GENETICS
doi: 10.1111/cge.12492

Short Report

Targeted next-generation sequencing in the diagnosis of neurodevelopmental disorders

Okamoto N., Miya F., Tsunoda T., Kato M., Saitoh S., Yamasaki M., Shimizu A., Torii C., Kanemura Y., Kosaki K.. Targeted next-generation sequencing in the diagnosis of neurodevelopmental disorders. Clin Genet 2014. © John Wiley & Sons A/S. Published by John Wiley & Sons Ltd, 2014

We developed a next-generation sequencing (NGS) based mutation screening strategy for neurodevelopmental diseases. Using this system, we screened 284 genes in 40 patients. Several novel mutations were discovered. Patient 1 had a novel mutation in *ACTB*. Her dysmorphic feature was mild for Baraitser-Winter syndrome. Patient 2 had a truncating mutation of *DYRK1A*. She lacked microcephaly, which was previously assumed to be a constant feature of *DYRK1A* loss of function. Patient 3 had a novel mutation in *GABRD* gene. She showed Rett syndrome like features. Patient 4 was diagnosed with Noonan syndrome with *PTPN11* mutation. He showed complete agenesis of corpus callosum. We have discussed these novel findings.

Conflict of interest

The authors report no conflicts of interest.

N. Okamoto[a], F. Miya[b], T. Tsunoda[b], M. Kato[c], S. Saitoh[d], M. Yamasaki[e], A. Shimizu[f], C. Torii[g], Y. Kanemura[h,i] and K. Kosaki[g]

[a]Department of Medical Genetics, Osaka Medical Center and Research Institute for Maternal and Child Health, Osaka, Japan, [b]Laboratory for Medical Science Mathematics, Center for Integrative Medical Sciences, RIKEN, Yokohama, Japan, [c]Department of Pediatrics, Yamagata University Faculty of Medicine, Yamagata, Japan, [d]Department of Pediatrics and Neonatology, Nagoya City University Graduate School of Medical Sciences, Nagoya, Japan, [e]Department of Pediatric Neurosurgery, Takatsuki General Hospital, Osaka, Japan, [f]Division of Biomedical Information Analysis, Iwate Tohoku Medical Megabank Organization, Iwate Medical University, Iwate, Japan, [g]Center for Medical Genetics, Keio University School of Medicine, Tokyo, Japan, [h]Division of Regenerative Medicine, Institute for Clinical Research, Osaka National Hospital, National Hospital Organization, Osaka, Japan, and [i]Department of Neurosurgery, Osaka National Hospital, National Hospital Organization, Osaka, Japan

Key words: Baraitser-Winter syndrome – *DYRK1A* – *GABRD* – next-generation sequencing

Corresponding author: Nobuhiko Okamoto, Department of Medical Genetics, Osaka Medical Center and Research Institute for Maternal and Child Health, 840, Murodo-cho, Izumi, Osaka 594-1101, Japan.
Tel.: +81 725 56 1220;
fax: +81 725 56 5682;
e-mail: okamoto@osaka.email.ne.jp

Received 26 April 2014, revised and accepted for publication 19 August 2014

Despite many recent studies focusing on discovering the genetic basis of neurodevelopmental diseases, it is still largely unknown. We developed a next-generation sequencing (NGS) based mutation screening strategy. We screened 284 genes known or predicted to be associated with neurodevelopmental disorders with microcephaly/macrocephaly, central nervous system (CNS) anomalies and intellectual disability (ID).

Materials and methods

We studied 40 patients with neurodevelopmental disorders. They were negative for conventional cytogenetic studies and microarray analysis. With the approval of our institutional ethics committee, the patients were analyzed using this targeted sequencing. The genomic DNA of each patient was extracted from peripheral blood using extraction kit. Detail of the cell sample preparation was described in Supporting information.

Target gene sequencing

Three microgram of each sample DNA was sheared to 150–200 bp using the Covaris DNA Shearing System (Wobum, MA, USA). To capture the target exonic DNA, we used the SureSelectXT Custom capture library (Agilent, Santa Clara, CA) for 1.6 Mb of exons of neuronal gene capture. The sequence library was constructed with the SureSelect XT Target Enrichment System for Illumina Paired-End Sequencing Library kit (Agilent) according to the manufacturer's instructions. We performed DNA sequencing of either 76- or 101-bp paired-end reads using the Illumina Genome Analyzer IIx (Illumina, San Diego, CA) and HiSeq 2000 sequencer (Illumina, San Diego, CA).

Single nucleotide variation (SNV) calling

NGS reads were aligned to the Human reference genome (GRCh37/hg19). We then excluded polymerase chain reaction (PCR) duplicates, and extracted reads uniquely mapped to the reference genome that were properly paired within the insert size within mean ± 2 standard deviation (SD) of the mean. Base calling was performed in on-target regions, those regions within 100 bp upstream and downstream of the exon capture probes. SNV and insertion and deletion (indel) calling were performed using SAM TOOLS and GATK software. We excluded known variants found in database. We then narrowed the candidates to only non-synonymous, nonsense and splice site SNVs and frame shift indels. More details of method for variant calling are described in Supporting information.

NGS base-call quality check

To analyze the quality of our base-calling algorithm, we used genotypes from HapMap database (release #28, obtained from ftp://ftp.ncbi.nlm.nih.gov/hapmap/genotypes/2010-08_phaseII+III/). Sanger sequence validation of SNVs was performed using Applied Biosystems 3730xl DNA Analyzer (Life Technologies, Carlsbad, CA).

Results

To identify the causal mutation for neuronal diseases, we designed custom capture probes for the exons of 284 neuronal genes (Table S1, Supporting information). We performed targeted genes sequencing using these probes and generated 1.7 Gb of sequence on average. The average read depth of the on-target regions was 608. To check the quality of our NGS base calls, we sequenced HapMap-JPT NA18943 using the same method as the other samples, and compared our NGS calls with the released genotype of the HapMap consortium. The genotypes for 3129 locations were comparable between the two data sets. All but 16 of the 3129 genotypes were concordant between our NGS calls and the HapMap data. We validated these mismatched 16 positions using Sanger sequencing and all 16 were consistent with our NGS calls (Tables S2 and S3). On the basis of this, we estimate the false positive and false negative rate of our SNV calling to be <0.032% (<1/3129).

Clinical reports

In all patients, developmental quotient (DQ) was measured using the Kyoto Scale of Psychological Development test.

Patient 1 with *ACTB* mutation

The 3-year-old female was born at 37 weeks of gestation by normal delivery. Her developmental milestones were markedly delayed. She sat unsupported at 18 months of age. Recently, she walked with support. She spoke several meaningful words. Her DQ was 39 at 2 years of age. Physical examination identified dysmorphic features, including a flat face, arched eyebrows, narrow palpebral fissures, low-set posteriorly rotated ears and a thin upper lip. Ophthalmological investigation revealed no colobomata. Her height was 86.3 cm (−0.8 SD), and weight was 12.3 kg (mean). Her head circumference was 50 cm (+1.2 SD) at 2 years and 6 months of age. Neuroradiological investigations revealed enlarged lateral ventricles, decreased white matter volume and pachygyria dominant in the frontal lobe (Fig. 1a,b).

A novel missense was identified in *ACTB*, c.733G>A, p.G245S. She was therefore diagnosed with Baraitser-Winter syndrome (BRWS) (1).

Patient 2 with *DYRK1A* mutation

The 7-year-old female patient was born at 39 weeks of gestation by induced delivery. Her developmental milestones were severely retarded. She could not walk independently. She had no communicative language. In addition, her visual acuity was disturbed by severe amblyopia. She could see and reach objects within 30 cm. She exhibited self-injurious behavior, temper tantrums and vocal tics by vibrating her palate. She

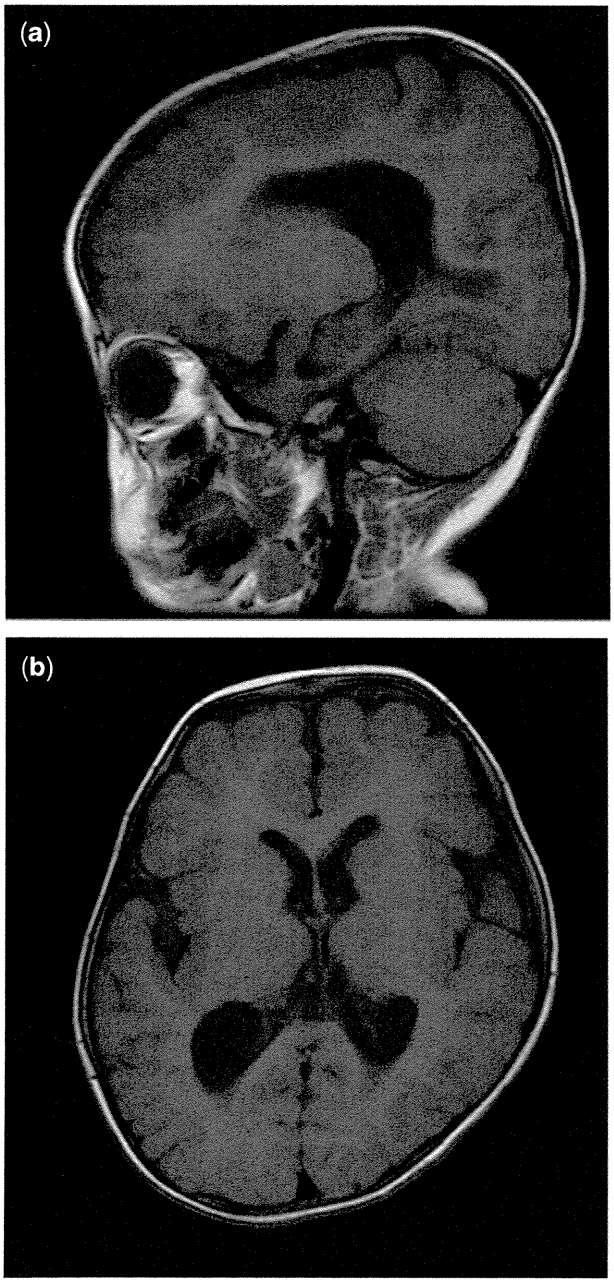

Fig. 1. (**a, b**) T1-weighted magnetic resonance image (MR) of patient 1 with *ACTB* mutation shows enlarged lateral ventricles, decreased white matter volume and pachygyria dominant in the frontal lobe.

was diagnosed with autism spectrum disorder (ASD) according to DSM-5. Her DQ was not properly assessed because of visual disturbance.

Physical examination identified dysmorphic features, including frontal bossing, hypertelorism, nystagmus, epicanthal folds, a flat nasal bridge, bilateral low-set ears, down-slanting palpebral fissures, a short philtrum, a high arched palate, downturned mouth and micrognathia. Her weight was 14.6 kg (−2.2 SD), height was 103.5 cm (−3.1 SD) and head circumference was 52 cm (+0.6 SD). She showed relative macrocephaly.

Brain computerized tomography (CT) and magnetic resonance imaging (MRI) were normal. Retinal abnormalities and optic nerve hypoplasia were not identified by fundoscopic investigations. Electroencephalography (EEG) showed no epileptic discharges. She had an early termination codon in exon 11 of the *DYRK1A* gene (c.C1699T: p.Q567*).

Patient 3 with *GABRD* mutation

The 12-year-old female was born at 41 weeks of gestation by induced delivery. Her development was severely retarded with generalized muscular hypotonia. She sat alone at 4 years of age. She cannot walk independently. She spoke no meaningful words. Her DQ was 12 at 9 years of age. She showed stereotyped behavior including hand gripping and bruxism. Purposeful hand skills were not obtained. She was diagnosed with Rett syndrome. EEG revealed bilateral occipital dominant high voltage slow spike and wave complex. Her height was 137 cm (−3.4 SD), weight was 35 kg (−2.1 SD) and head circumference was 51 cm (−1.8 SD). Brain CT and MRI were normal.

She had 2 bp insertion–deletion corresponding to two amino acids in *GABRD* gene (c.G498A:p.M166I and, c.G499A: p.D167N) (Fig. 2). This mutation was *de novo*.

Patient 4 with *PTPN11* mutation

The 4-year-old male was born at 40 weeks of gestation by normal delivery. Profound sensorineural hearing loss was confirmed. He was able to control his head at 4 months, roll over at 6 months of age. He could sit without support at 14 months of age. He started to walk without support at 3 years of age. His height was 90.7 cm (−1.8 SD), weight was 14.3 kg (−0.4 SD) and head circumference was 48.3 cm (−1.1 SD). Brain MRI at 4 years of age showed agenesis of corpus callosum (ACC) (Fig. 3). His DQ was 40. His dysmorphic features including hypertelorism, epicanthal folds, flat nasal bridge, low set ears, growth failure and ACC suggested the diagnosis of Mowat-Wilson syndrome. However, molecular analysis of *ZEB2* mutation was negative. Target gene sequencing revealed a heterozygous mutation in the *PTPN11* gene (c.A188G, p.Y63C). This mutation has been repeatedly reported in Noonan syndrome (NS) (2). We reevaluated his clinical features and concluded that the diagnosis of NS is appropriate. This is the first association of ACC and NS with *PTPN11* mutation.

Other patients

Three patients with cerebellar anomalies were diagnosed with mental retardation and microcephaly with pontine and cerebellar hypoplasia (MICPCH) due to *CASK* mutations. Another patient was homozygous for *AHI1* mutation. The diagnosis of Joubert syndrome was confirmed. They showed typical findings.

Discussion

ACTB mutation in patient 1 was predicted to be pathogenic in *in silico* analysis. BRWS is a rare

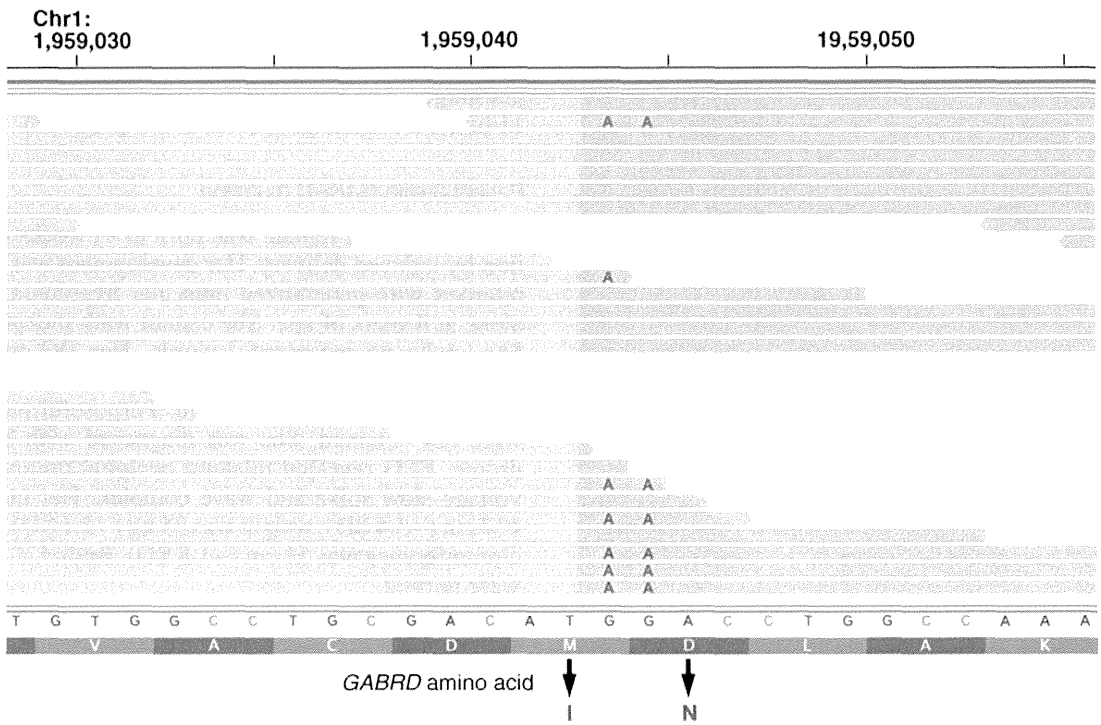

Fig. 2. Patient 3 had 2 bp insertion–deletion corresponding to two amino acids in *GABRD* gene (NM_000815: exon5: c.G498A: p.M166I and NM_000815: exon5: c.G499A: p.D167N).

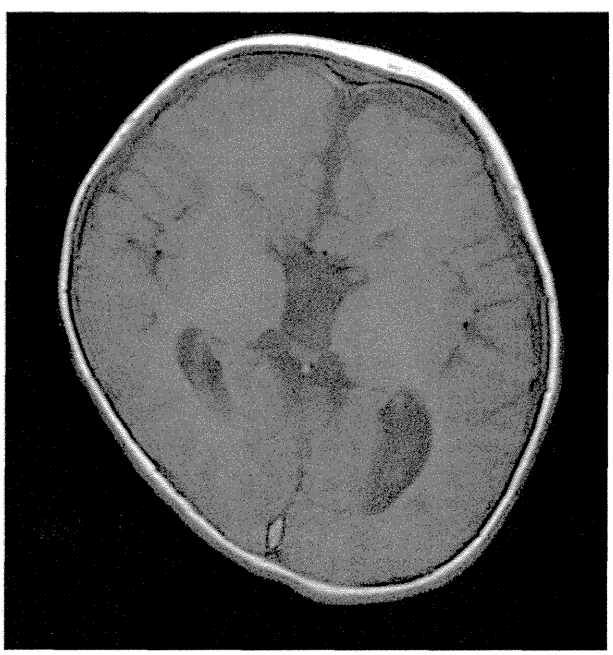

Fig. 3. Brain magnetic resonance imaging (MRI) of patient 4 with *PTPN11* mutation showed agenesis of corpus callosum

MCA/ID syndrome characterized by dysmorphic features, including ptosis, colobomata and neuronal migration anomalies (1). Rivière et al. (3) reported that mutations in *ACTB* and *ACTG1* cause BRWS. Clinical variability of BRWS is often discussed. Di Donato et al. (4) reported three patients with Fryns-Aftimos syndrome (FAS) who had a mutation in the *ACTB* gene. They suggested that mutations in *ACTB* cause a distinctly more severe phenotype than *ACTG1* mutations. They concluded that FAS is an early and severe manifestation of BRWS. Patient 1 did not show the typical features of BRWS. Her dysmorphic features were mild, and her head circumference was over average size. Recently, Verloes et al. (5) delineated the spectrum in 42 patients with BRWS. They reported that facial dysmorphism varies from mild to severe and evolves considerably over times. They suggested the designation of Baraitser-Winter cerebrofrontofacial syndrome.

Patient 2 had had severe ID, motor disturbance, autistic behavior and visual problems. She had truncating mutation of *DYRK1A*. She lacked microcephaly, which was previously assumed to be a constant feature of *DYRK1A* loss of function. *DYRK1A* is a protein kinase that belongs to the highly conserved dual-specificity tyrosine phosphorylation-regulated kinase (DYRK) family. *DYRK1A* is a highly conserved gene located in the Down syndrome critical region at 21q22. *DYRK1A* is involved in brain growth through neuronal proliferation and neurogenesis. *DYRK1A* overexpression has been implicated in ID and microcephaly in Down syndrome.

Haploinsufficiency of *DYRK1A* is associated with ID, epilepsy and microcephaly (6). So far, mutation analysis of *DYRK1A* has been carried out in patients with ID and microcephaly (7, 8). Courset et al. (9) studied the *DYRK1A* gene in a cohort of 105 patients with ID and Angelman syndrome-like symptoms, and they identified a *de novo* frameshift mutation in a patient with growth retardation, ID, and seizures. O'Roak et al. (10)

captured and sequenced 44 candidate genes in 2446 ASD probands. They discovered 27 *de novo* events in 16 genes including *DYRK1A*. The three patients with a *DYRK1A* mutation showed microcephaly.

We suppose that the clinical spectrum of *DYRK1A* mutations may have more variability. Microcephaly may not be a constant feature in the patients with *DYRK1A* mutations. Another novel finding in patient 2 was severe amblyopia. *Dyrk1A* (+/−) mice showed thin retina (11). We recommend ophthalmologic investigation for patients with *DYRK1A* mutations.

Patient 3 had a 2 bp insertion–deletion corresponding to two amino acids in *GABRD* gene. This is the first report of a *GABRD* mutation associated with Rett syndrome like features. *GABRD* encodes a subunit of the ligand-gated chloride channel for gamma-aminobutyric acid (GABA), the major inhibitory neurotransmitter (12). The majority of GABAA receptors contain two α-subunits, two β-subunits, and a γ- or δ-subunit. Mutations in inhibitory GABAA receptor subunit genes (*GABRA1*, *GABRB3*, *GABRG2* and *GABRD*) have been associated with genetic epilepsy syndromes including childhood absence epilepsy (CAE), juvenile myoclonic epilepsy (JME), pure febrile seizures (FS), generalized epilepsy with febrile seizures plus (GEFS+), and Dravet syndrome (or severe myoclonic epilepsy in infancy).

There have been some reports on the association of generalized epilepsies and *GABRD* mutations. *GABRD* gene is assigned to chromosome 1p36 (13). Patients with the 1p36 deletion syndrome often have epileptic seizures (14). Windpassinger et al. (12) found that *GABRD* is expressed most abundantly in the brain. They suggested that the *GABRD* is a good candidate for the neurodevelopmental and neuropsychiatric anomalies seen in the 1p36 deletion syndrome.

Patient 3 has been diagnosed with Rett syndrome. Heterozygous disruption of *GABRB3* produces increased epileptiform EEG activity and elevated seizure susceptibility in Angelman syndrome (15). We assume that mutant *GABRD* is likely to cause increased neuronal excitability in our patient. Further investigation is necessary to clarify mutations in Rett syndrome-like patients without known genetic causes.

Patient 4 was diagnosed with NS, the most common RASopathy characterized by short stature, distinct facial features, congenital heart defect, and ID of various degrees. Patient 4 showed ACC. So far association of NS and ACC is not known. Hypoplasia of corpus callosum is occasionally reported in cardio-facio-cutaneous syndrome, another RASopathy. We consider ACC to be an unusual manifestation of RASopathy.

Our NGS-based mutation screening strategy showed a certain success in the diagnosis of patients with neurodevelopmental disorders when conventional clinical genetic testing has proven negative. Presented patients showed unique or unexpected manifestations. We are planning whole-exome sequencing for the remaining unexplained patients.

Supporting Information

Additional supporting information may be found in the online version of this article at the publisher's web-site.

Acknowledgements

This study was supported by a grant from the Research on Applying Health Technology from the Ministry of Health, Labor and Welfare of Japan. We thank the patients and their families for participating in this work. We thank Mr K. A. Boroevich for English proofreading.

References

1. Baraitser M, Winter RM. Iris coloboma, ptosis, hypertelorism, and mental retardation: a new syndrome. J Med Genet 1988: 25: 41–43.
2. Tartaglia M, Mehler EL, Goldberg R et al. Mutations in PTPN11, encoding the protein tyrosine phosphatase SHP-2, cause Noonan syndrome. Nat Genet 2001: 29: 465–468.
3. Rivière JB, van Bon BW, Hoischen A et al. De novo mutations in the actin genes ACTB and ACTG1 cause Baraitser-Winter syndrome. Nat Genet 2012: 44: 440–444.
4. Di Donato N, Rump A, Koenig R et al. Severe forms of Baraitser-Winter syndrome are caused by ACTB mutations rather than ACTG1 mutations. Eur J Hum Genet 2014: 22: 179–183.
5. Verloes A, Di Donato N, Masliah-Planchon J et al. Baraitser-Winter cerebrofrontofacial syndrome: delineation of the spectrum in 42 cases. Eur J Hum Genet 2014 Jul 23. doi: 10.1038/ejhg.2014.95. [Epub ahead of print]
6. Moller RS, Kubart S, Hoeltzenbein M et al. Truncation of the Down syndrome candidate gene DYRK1A in two unrelated patients with microcephaly. Am J Hum Genet 2008: 82: 1165–1170.
7. Yamamoto T, Shimojima K, Nishizawa T et al. Clinical manifestations of the deletion of Down syndrome critical region including DYRK1A and KCNJ6. Am J Med Genet A 2010: 155A: 113–119.
8. Valetto A, Orsini A, Bertini V et al. Molecular cytogenetic characterization of an interstitial deletion of chromosome 21 (21q22.13q22.3) in a patient with dysmorphic features, intellectual disability and severe generalized epilepsy. Eur J Med Genet 2012: 55: 362–366.
9. Courcet JB, Faivre L, Malzac P et al. The DYRK1A gene is a cause of syndromic intellectual disability with severe microcephaly and epilepsy. J Med Genet 2012: 49: 731–736.
10. O'Roak BJ, Vives L, Fu W, Egertson JD et al. Multiplex targeted sequencing identifies recurrently mutated genes in autism spectrum disorders. Science 2012: 338: 1619–1622.
11. Laguna A, Barallobre MJ, Marchena MÁ et al. Triplication of DYRK1A causes retinal structural and functional alterations in Down syndrome. Hum Mol Genet 2013: 22: 2775–2784.
12. Windpassinger C, Kroisel PM, Wagner K et al. The human gamma-aminobutyric acid A receptor delta (GABRD) gene: molecular characterisation and tissue-specific expression. Gene 2002: 292: 25–31.
13. Emberger W, Windpassinger C, Petek E et al. Assignment of the human GABAA receptor delta-subunit gene (GABRD) to chromosome band 1p36.3 distal to marker NIB1364 by radiation hybrid mapping. Cytogenet Cell Genet 2000: 89: 281–282.
14. Rosenfeld JA, Crolla JA, Tomkins S et al. Refinement of causative genes in monosomy 1p36 through clinical and molecular cytogenetic characterization of small interstitial deletions. Am J Med Genet A 2010: 152A: 1951–1959.
15. DeLorey TM, Olsen RW. GABA and epileptogenesis: comparing gabrb3 gene-deficient mice with Angelman syndrome in man. Epilepsy Res 1999: 36: 123–132.

Published online: January 15, 2015

Research Article

SOURCE DATA | TRANSPARENT PROCESS | OPEN ACCESS

EMBO Molecular Medicine

An aberrant sugar modification of BACE1 blocks its lysosomal targeting in Alzheimer's disease

Yasuhiko Kizuka[1], Shinobu Kitazume[1,*], Reiko Fujinawa[1], Takashi Saito[2], Nobuhisa Iwata[2,3], Takaomi C Saido[2], Miyako Nakano[4], Yoshiki Yamaguchi[5], Yasuhiro Hashimoto[6], Matthias Staufenbiel[7], Hiroyuki Hatsuta[8], Shigeo Murayama[8], Hiroshi Manya[9], Tamao Endo[9] & Naoyuki Taniguchi[1,**]

Abstract

The β-site amyloid precursor protein cleaving enzyme-1 (BACE1), an essential protease for the generation of amyloid-β (Aβ) peptide, is a major drug target for Alzheimer's disease (AD). However, there is a concern that inhibiting BACE1 could also affect several physiological functions. Here, we show that BACE1 is modified with bisecting N-acetylglucosamine (GlcNAc), a sugar modification highly expressed in brain, and demonstrate that AD patients have higher levels of bisecting GlcNAc on BACE1. Analysis of knockout mice lacking the biosynthetic enzyme for bisecting GlcNAc, GnT-III (*Mgat3*), revealed that cleavage of Aβ-precursor protein (APP) by BACE1 is reduced in these mice, resulting in a decrease in Aβ plaques and improved cognitive function. The lack of this modification directs BACE1 to late endosomes/lysosomes where it is less colocalized with APP, leading to accelerated lysosomal degradation. Notably, other BACE1 substrates, CHL1 and contactin-2, are normally cleaved in GnT-III-deficient mice, suggesting that the effect of bisecting GlcNAc on BACE1 is selective to APP. Considering that GnT-III-deficient mice remain healthy, GnT-III may be a novel and promising drug target for AD therapeutics.

Keywords Alzheimer's disease; amyloid-β; BACE1; bisecting GlcNAc; GnT-III
Subject Category Neuroscience
DOI 10.15252/emmm.201404438 | Received 4 August 2014 | Revised 2 December 2014 | Accepted 12 December 2014 | Published online 15 January 2015
EMBO Mol Med (2015) 7: 175–189

Introduction

Alzheimer's disease (AD) is a devastating dementia, with the number of patients now estimated to be ~0.5% of the global population (Abbott, 2011; Selkoe, 2012). Deposition of amyloid-β (Aβ) peptide in the brain is considered to represent the initial event in disease development (Karran *et al*, 2011). Aβ is generated by the two-step proteolytic cleavage of amyloid precursor protein (APP), which is catalyzed by the β-site APP cleaving enzyme-1 (BACE1, also designated as β-secretase) (Vassar *et al*, 2014) and γ-secretase (De Strooper & Annaert, 2010). However, when APP is cleaved at the α-site within the Aβ sequence by α-secretase, pathogenic Aβ is not generated. Current trials to develop γ-secretase inhibitors have been unsuccessful due to serious side effects, probably as a result of disturbing the signaling of Notch (De Strooper *et al*, 1998), another substrate for γ-secretase. BACE1 protease also has substrates other than APP (Kuhn *et al*, 2012; Vassar *et al*, 2014), including α2,6-sialyltransferase (Kitazume *et al*, 2001), P-selectin glycoprotein ligand-1 (PSGL-1) (Lichtenthaler *et al*, 2003), APP homolog proteins (APLP1 and APLP2) (Eggert *et al*, 2004; Li & Sudhof, 2004; Pastorino *et al*, 2004), low-density lipoprotein receptor-related protein (LRP) (von Arnim *et al*, 2005), voltage-gated sodium channel (Na_v1) β subunits (Kim *et al*, 2005; Wong *et al*, 2005), neuregulins 1 and 3 (NRG1, 3) (Hu *et al*, 2006; Willem *et al*, 2006), and neural cell adhesion molecules (L1 and CHL1) (Zhou *et al*, 2012). *Bace1*$^{-/-}$ mice display retinal pathology (Cai *et al*, 2012) and changes in NRG1 signaling, leading to a schizophrenia-like phenotype (Savonenko *et al*, 2008) and impaired formation of muscle spindles (Cheret *et al*, 2013). This indicates that BACE1 also has physiological roles in addition to its involvement in the pathogenesis of AD.

Increasing evidence shows that aberrant glycosylation is a critical factor for the development of various diseases (Dennis *et al*, 2009; Godfrey *et al*, 2011; Ohtsubo *et al*, 2005). Lack of glycosylation causes dysfunction of target glycoproteins, including impaired glycoprotein folding (Hebert *et al*, 2005), poor ligand binding of a receptor glycoprotein (Wang *et al*, 2005), or shortened cell surface retention of a glycoprotein (Dennis *et al*, 2009; Ohtsubo *et al*,

1 Disease Glycomics Team, RIKEN-Max Planck Joint Research Center, Global Research Cluster, RIKEN, Wako, Japan
2 Laboratory for Proteolytic Neuroscience, RIKEN Brain Science Institute, Wako, Japan
3 Department of Genome-based Drug Discovery, Unit of Molecular Medicinal Sciences, Graduate School of Biomedical Sciences, Nagasaki University, Nagasaki, Japan
4 Graduate School of Advanced Sciences of Matter, Hiroshima University, Higashihiroshima, Hiroshima, Japan
5 Structural Glycobiology Team, RIKEN-Max Planck Joint Research Center, Global Research Cluster, RIKEN, Wako, Japan
6 Department of Biochemistry, Fukushima Medical University School of Medicine, Fukushima, Japan
7 Novartis Institutes for Biomedical Research, Basel, Switzerland
8 Department of Neuropathology, Research Team for Mechanism of Aging, Tokyo Metropolitan Geriatric Hospital and Institute of Gerontology, Itabashi-ku, Tokyo, Japan
9 Molecular Glycobiology, Research Team for Mechanism of Aging, Tokyo Metropolitan Geriatric Hospital and Institute of Gerontology, Itabashi-ku, Tokyo, Japan
*Corresponding author. Tel: +81 48 467 9616; Fax: +81 48 467 9617; E-mail: shinobuk@riken.jp
**Corresponding author. Tel: +81 48 467 9616; Fax: +81 48 467 9617; E-mail: dglycotani@riken.jp

2005). Although the roles of glycans in AD pathology remain unclear, most AD-related molecules, including APP and its secretases (a disintegrin and metalloproteinases (ADAMs) and BACE1), carry glycans, highlighting the possibility that Aβ generation could be regulated by their glycosylation.

Here, we focus on bisecting N-acetylglucosamine (GlcNAc), a unique *N*-glycan structure that is highly expressed in the brain (Fig 1A). Although this sugar modification has been suggested to suppress cancer metastasis (Taniguchi *et al*, 2006), its target glycoprotein and the function of bisecting GlcNAc in the brain have not been explored. We have previously found that the glycosyltransferase, GnT-III (encoded by the *MGAT3* gene) (Nishikawa *et al*, 1992), which is the sole biosynthetic enzyme for bisecting GlcNAc modification (Bhattacharyya *et al*, 2002), is upregulated in the brains of AD patients (Akasaka-Manya *et al*, 2010), but how this increase in bisected glycan contributes to AD pathology remained unclear. In this study, we have identified BACE1 as a novel *in vivo* target glycoprotein for this modification. By analyzing the brains of GnT-III (*Mgat3*)-deficient mice, we demonstrate that the sugar modification promotes AD pathogenesis by delaying BACE1 degradation. Considering that *Mgat3*$^{-/-}$ mice show almost no phenotypic abnormality in terms of development, reproduction, hematology, and brain morphology (Orr *et al*, 2013; Priatel *et al*, 1997), our results highlight the possibility of a novel strategy for developing glycosyltransferase-targeted AD therapeutics.

Results

AD patients have higher levels of bisecting GlcNAc on BACE1

We have previously found that a GlcNAc-transferase GnT-III (encoded by *MGAT3*) that generates bisecting GlcNAc is upregulated in AD brains (Akasaka-Manya *et al*, 2010). We also found, using a lectin E4-phytohemagglutinin (PHA) for detection (Cummings & Kornfeld, 1982) (Supplementary Fig S1A and B), that

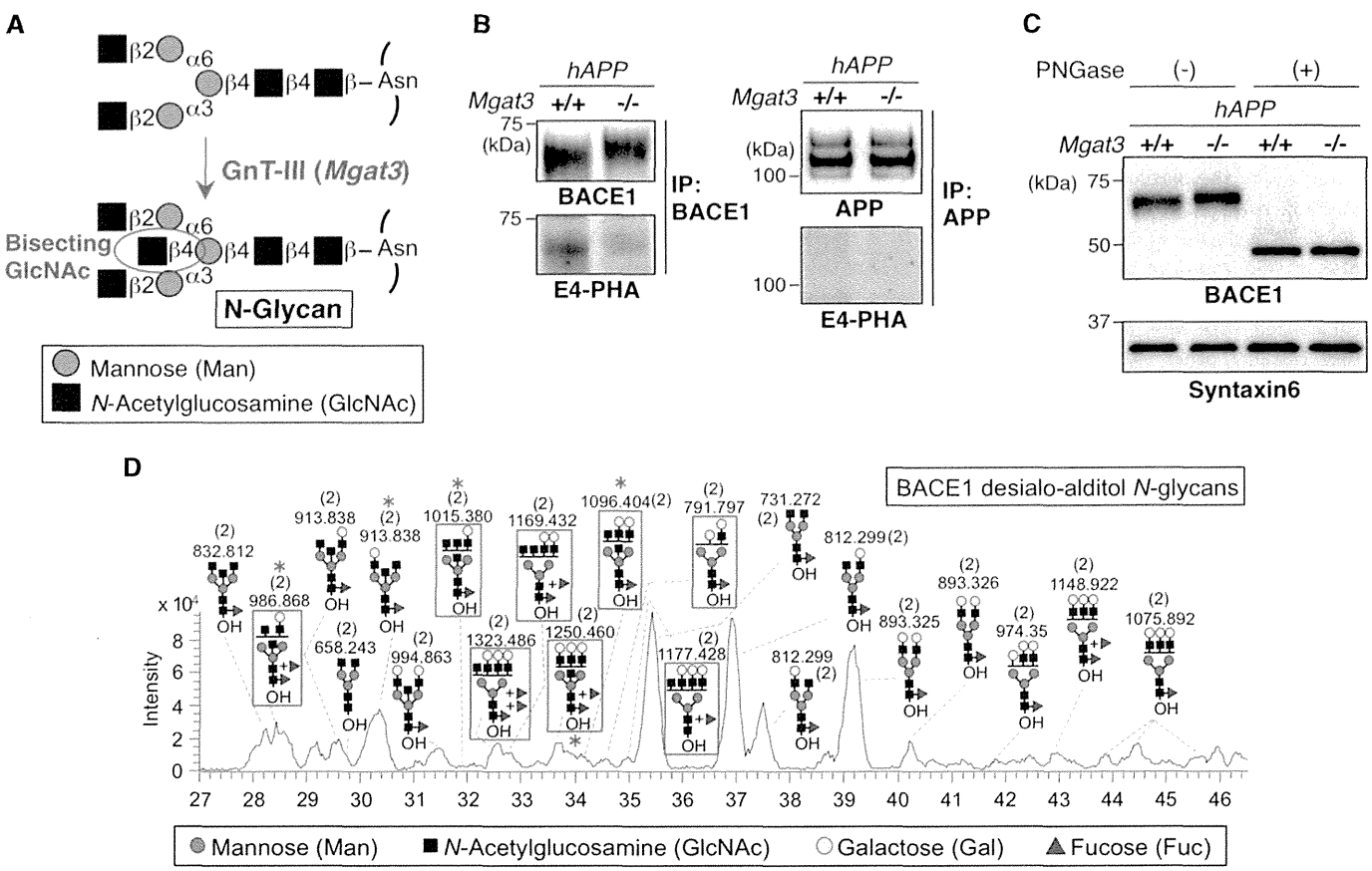

Figure 1. BACE1 is modified with bisecting GlcNAc *in vivo*.

A Bisecting GlcNAc modification by GnT-III.

B BACE1 or APP was immunoprecipitated from mouse brains and blotted with E4-PHA lectin (lower) or anti-BACE1 or APP antibodies (upper). *hAPP* indicates the APP23 transgenic mouse model for AD.

C Proteins from mouse brain membrane fractions were treated with or without PNGase F and then immunoblotted for BACE1 or for syntaxin 6 (loading control).

D LC–MS base peak chromatogram of desialo-alditol *N*-glycans derived from mouse brain BACE1. To simplify the results, *N*-glycans were chemically desialylated before LC–MS analysis. BACE1-specific glycans, judged by comparison with *N*-glycan structures from anti-BACE1 IgG (shown in Supplementary Fig S2C), are highlighted by red squares. Asterisks indicate glycans demonstrated by MS/MS analysis to contain a bisecting GlcNAc structure. Numbers in parentheses indicate the charge state.

Source data are available online for this figure.

bisecting GlcNAc is mainly expressed in neurons (Supplementary Fig S1C). From these results, we hypothesized that a key molecule involved in AD pathogenesis is modified with this sugar chain to modulate disease progression. We first found a clear mobility shift of BACE1 but not APP in response to GnT-III deficiency (Fig 1B), even after the enzymatic removal of O-glycans from APP (Supplementary Fig S1D). We also demonstrated that BACE1 but not APP was recognized by E4-PHA lectin (Fig 1B lower panels and Supplementary Fig S1E). The reactivity of E4-PHA to BACE1 was largely absent in GnT-III-deficient ($Mgat3^{-/-}$) mice. We confirmed that APP was modified with bisecting GlcNAc in C17 neuroblastoma cells (Akasaka-Manya *et al*, 2008), while APP in the brain was not reactive with E4-PHA (Supplementary Fig S1F), suggesting that modification of APP with bisecting GlcNAc occurs in a limited number of cell types (Kitazume *et al*, 2010) and is non-existent or negligible in the brain. In addition, we found that nicastrin, the only glycosylated subunit of γ-secretase, was slightly modified with bisecting GlcNAc (Supplementary Fig S1G) in spite of the presence of 16 possible *N*-glycosylation sites. In light of these results, as well as several previous reports showing that a change in the glycosylation of nicastrin does not affect γ-secretase activity (Herreman *et al*, 2003; Schedin-Weiss *et al*, 2014), we suggest that BACE1 is a likely functional target of bisecting GlcNAc modification in the Aβ-generation pathway.

The mobility difference in BACE1 disappeared after cleavage of *N*-glycans by peptide:*N*-glycanase (PNGase) F (Fig 1C). Furthermore, based on MS/MS analysis of *N*-glycans released from the BACE1 immunopurified from mouse brains (Fig 1D; Supplementary Fig S2A–C), we detected diagnostic ions derived from bisecting GlcNAc-containing glycans (Supplementary Fig S2D–H), clearly demonstrating the presence of bisecting GlcNAc on BACE1 *N*-glycans (Fig 1D, asterisk). These results indicate that BACE1 is selectively modified with bisecting GlcNAc by GnT-III on its *N*-glycan *in vivo*.

We assumed that the level of bisecting GlcNAc on BACE1 would be increased with disease progression. To test this, BACE1 was immunoprecipitated from the temporal lobe of non-AD, early-stage AD, and late-stage AD patients and then blotted with E4-PHA (Fig 2). The lectin reactivity to BACE1 started to increase in early-stage AD. This indicates that the level of bisecting GlcNAc on BACE1 is elevated with disease progression in the human brain, suggesting that this abnormal change in BACE1 glycosylation is involved in AD pathogenesis by modulating β-site cleavage of APP.

Loss of bisecting GlcNAc reduces Aβ generation and ameliorates AD pathology in mice

To investigate how bisecting GlcNAc affects the metabolic pathway of APP *in vivo*, we analyzed APP metabolites in $Mgat3^{-/-}$ mice crossed with AD model mice expressing human APP (designated *hAPP*, the APP23 transgenic mouse model for AD). Western blot of APP and its cleaved fragments clearly showed that $hAPP/Mgat3^{-/-}$ mice had significantly lower levels of the β-C-terminal fragment of APP (βCTF) and soluble APP cleaved at the β-site (sAPPβ) in their brains than $hAPP/Mgat3^{+/+}$ mice, whereas the levels of full-length

A

		Gender		Clinical dementia rating				Braak				CERAD*			
	Age	M	F	N/A	0	0.5	≧1	NFT	Aβ 0	Aβ B	Aβ C	0	1	2	3
AD	88.2 ± 6.73	6	4	0	0	0	10	V - VI	0	0	10	0	0	0	10
Early AD	90.3 ± 6.38	5	5	1	0	4	5	III	0	6	4	0	3	5	2
Non-AD	75.8 ± 6.00	7	3	2	7	0	1	≤ II	10	0	0	10	0	0	0

*CERAD: Consortium to Establish a Registry for Alzheimer's Disease

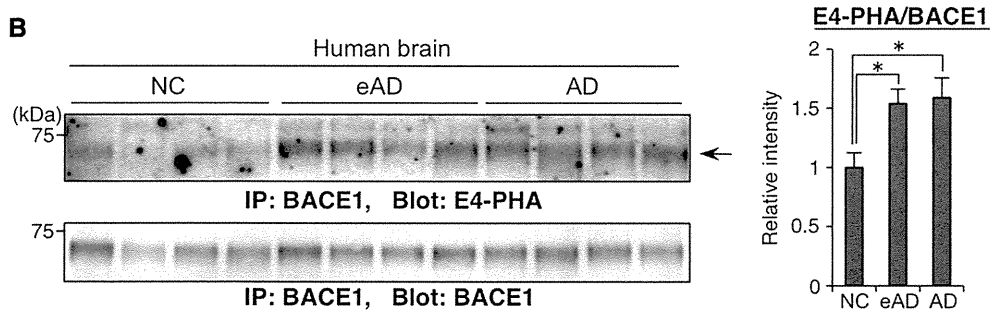

Figure 2. BACE1 is abnormally hyper-modified with bisecting GlcNAc in AD patients.

A Summary of clinical and histological data of non-AD control (NC), early-stage AD (eAD) or AD patients.

B BACE1 from temporal lobe membrane fractions of NC, eAD, or AD patients was immunoprecipitated and blotted with E4-PHA (upper) or anti-BACE1 (lower). The signal intensity of E4-PHA relative to that of BACE1 was calculated (n = 10). The graph shows means ± SEM (*P < 0.05; one-way ANOVA with *post hoc* Tukey–Kramer test. P = 0.014 for NC versus eAD, P = 0.028 for NC versus AD).

Source data are available online for this figure.

APP, αCTF, and sAPPα were comparable (Fig 3), suggesting that bisecting GlcNAc on BACE1 plays a critical role in the β-cleavage process.

We next measured the steady-state levels of Aβ40 and Aβ42 (the two major isoforms of Aβ) in 3- and 12-month-old mouse brains. In *hAPP/Mgat3*$^{+/+}$ mice, both Aβ40 and Aβ42 levels increased in an age-dependent manner (Fig. 4A and B), whereas the amounts of Aβ40/42 in both the Tris-buffered saline (TBS)-soluble and guanidine (Gu)-HCl-extractable fractions were significantly reduced in the *hAPP/Mgat3*$^{-/-}$ mouse brains, consistent with the impairment of β-cleavage by GnT-III deficiency. It should also be noted that a prominent Aβ reduction was observed in 12-month-old mice and that *hAPP/Mgat3*$^{+/-}$ mice displayed Aβ levels that were intermediate between those of *hAPP/Mgat3*$^{+/+}$ and *hAPP/Mgat3*$^{-/-}$ mice. We also confirmed a slight but significant reduction in Aβ levels in non-APP-transgenic *Mgat3*$^{-/-}$ mice (Fig 4C), excluding the possibility that the Aβ reduction by GnT-III deficiency is an APP-transgenic mouse-specific phenomenon. Immunohistochemical analysis revealed that the number of Aβ plaques was markedly decreased in the *hAPP/Mgat3*$^{-/-}$ mice (Fig 4D), and the synaptic loss and accumulation of activated astrocytes around Aβ plaques (Saito *et al*, 2014) observed in *hAPP/Mgat3*$^{+/+}$ mouse brains were either absent or reduced in *hAPP/Mgat3*$^{-/-}$ brains (Supplementary Fig S3). Moreover, cognitive impairment in *hAPP/Mgat3*$^{+/+}$ mice as measured by the Y-maze test was significantly rescued in *hAPP/Mgat3*$^{-/-}$ mice (Fig 4E). These results show that deletion of bisecting GlcNAc ameliorates AD-related abnormalities through reduced Aβ deposition caused by impaired β-cleavage.

BACE1 is more localized to late endosomes/lysosomes, leading to accelerated degradation of BACE1 in Mgat3-deficient mice

One possible explanation for the reduced β-cleavage in *hAPP/Mgat3*$^{-/-}$ brain is that bisecting GlcNAc on BACE1 affects its catalytic activity. We therefore measured the *in vitro* enzymatic activity of BACE1 with or without bisecting GlcNAc using fluorescently labeled APP-derived peptide. Immunoprecipitated BACE1 from *Mgat3*$^{+/+}$ and *Mgat3*$^{-/-}$ mouse brains showed comparable enzymatic activity *in vitro* (Fig 5A). Likewise, overexpression of either GnT-III or dominant negative GnT-III had no effect on the enzymatic activity of recombinant BACE1-Fc (Supplementary Fig S4A and B). In addition, a docking model of the tertiary structure of BACE1 with bisected *N*-glycans showed that all glycans lie apart from the catalytic center (Supplementary Fig S4C). Therefore, it is unlikely that the enzymatic activity of BACE1 is directly modulated by bisecting GlcNAc, although it is still possible that glycans exposed at the molecular surface exert an indirect effect due to the impaired dimerization of BACE1 (Schmechel *et al*, 2004; Westmeyer *et al*, 2004).

We then hypothesized that loss of bisecting GlcNAc results in abnormal subcellular localization of BACE1, leading to the marked reduction in Aβ generation in cells. To test this, we prepared mouse embryonic fibroblasts (MEFs) from *Mgat3*$^{+/+}$ and *Mgat3*$^{-/-}$ mice and performed subcellular fractionation of BACE1 and APP by sucrose density gradient centrifugation. We found that BACE1 in *Mgat3*$^{+/+}$ MEFs was mainly co-distributed with an early endosome marker and APP, whereas in *Mgat3*$^{-/-}$ cells, BACE1 showed a different distribution from that of APP (Fig 5B). This altered localization of BACE1 but not of APP was also found in 3-month-old (Fig 5C) and 12-month-old *hAPP/Mgat3*$^{-/-}$ brains (Supplementary Fig S4D), although the difference was less than that observed in *Mgat3*$^{-/-}$MEFs. Immunostaining of mouse brain sections showed that co-localization of BACE1 and APP was significantly reduced in the *hAPP/Mgat3*$^{-/-}$ brain (Fig 5D). It was recently reported that BACE1 is localized in endosomal compartments to cleave APP (Das *et al*, 2013), and we confirmed that degradation of BACE1 protein occurs mainly in lysosomes (Koh *et al*, 2005) but not in the proteasome (Fig 5E). We therefore expected that, in the absence of bisecting GlcNAc, BACE1 would relocate to late endosomes/lysosomes. Indeed, we found that BACE1 in the brains of *hAPP/Mgat3*$^{-/-}$ mice was more co-localized with the late endosome/lysosome marker Lamp1 than in *hAPP/Mgat3*$^{+/+}$ mice (Fig 5F). We also stained nicastrin as a control protein and confirmed that co-localization of nicastrin with Lamp1 was not altered in *hAPP/Mgat3*$^{+/+}$ mice (Fig 5G). Similarly, immunofluorescence staining of *Mgat3*$^{-/-}$ primary neurons revealed increased co-localization of BACE1 but not nicastrin with Lamp1 compared with the pattern in *Mgat3*$^{+/+}$ neurons (Supplementary Fig S4E and F).

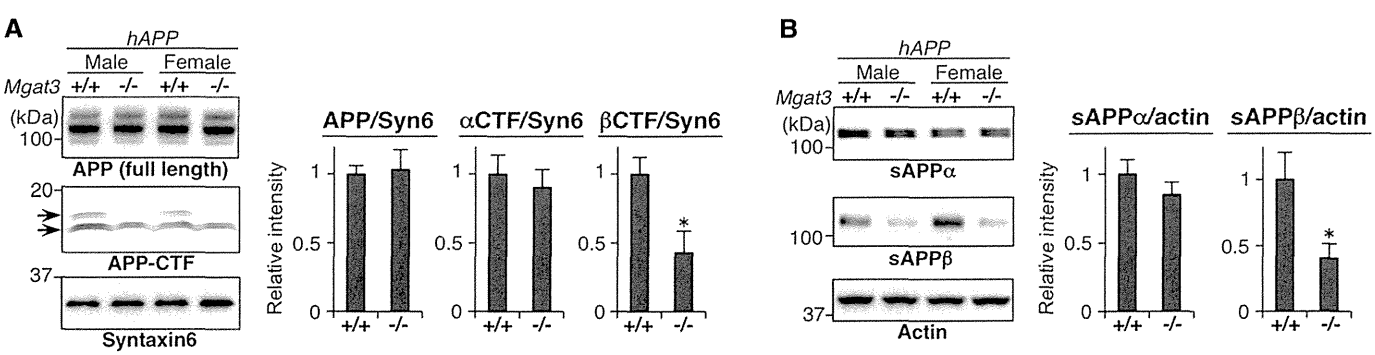

Figure 3. Impaired β-site cleavage of APP in *Mgat3*$^{-/-}$ brain.

A, B APP metabolites from 3-month-old mouse brain membrane (A) or soluble (B) fractions were immunoblotted. The signal intensity was quantified (n = 4–5). All graphs show means ± SEM (*P < 0.05; Student's t-test for (A) βCTF and (B) sAPPα, and Mann–Whitney U-test for the others. P = 0.386 for APP, P = 0.602 for αCTF, P = 0.045 for βCTF, P = 0.218 for sAPPα, P = 0.022 for sAPPβ).

Source data are available online for this figure.

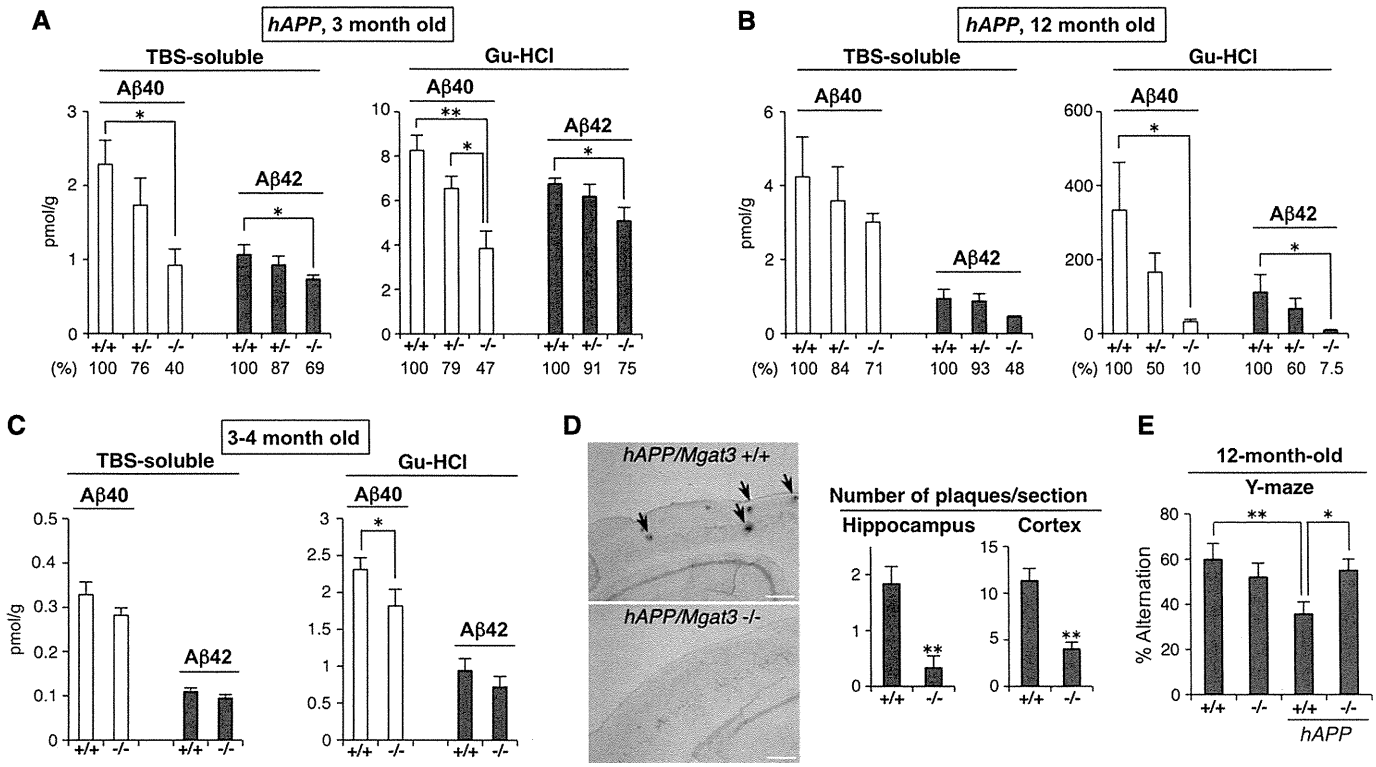

Figure 4. Reduced Aβ load and ameliorated cognitive function in *Mgat3*$^{-/-}$ mouse brain.

A, B Amounts of Aβ40 or Aβ42 in the TBS-soluble or Gu-HCl-extractable fraction from (A) 3-month-old or (B) 12-month-old *hAPP/Mgat3*$^{+/+}$, *hAPP/Mgat3*$^{+/-}$, or *hAPP/Mgat3*$^{-/-}$ brains (n = 5). P = 0.015 for TBS Aβ40, P = 0.034 for TBS Aβ42, P = 0.001 and 0.012 for Gn–HCl Aβ40, P = 0.024 for Gn–HCl Aβ42 in (A), P = 0.040 for Gn–HCl Aβ40, P = 0.047 for Gn–HCl Aβ42 in (B).

C Amounts of Aβ40 or Aβ42 in the TBS-soluble or Gu-HCl-extractable fraction from 3- to 4-month-old *Mgat3*$^{+/+}$ or *Mgat3*$^{-/-}$ brains (n = 7–8). An outlier value was rejected by the Smirnov–Grubbs' test (P < 0.05). P = 0.045 for Gn–HCl Aβ40.

D Immunostaining of Aβ plaques in 12-month-old mouse brain (left). Scale bar, 300 μm. The number of FSB-stained Aβ plaques in brain sections prepared from 12-month-old male mice was quantified (right) (n = 6). P = 0.004 for hippocampus, P = 0.0003 for cortex.

E The Y-maze test was performed using 12-month-old male *Mgat3*$^{+/+}$, *Mgat3*$^{-/-}$, *hAPP/Mgat3*$^{+/+}$, or *hAPP/Mgat3*$^{-/-}$ mice (n = 8–10). **P = 0.004 for *Mgat3*$^{+/+}$ versus *hAPP/Mgat3*$^{+/+}$, *P = 0.022 for *hAPP/Mgat3*$^{+/+}$ versus *hAPP/Mgat3*$^{-/-}$.

Data information: All graphs show means ± SEM (*P < 0.05, **P < 0.01. For comparison between two groups, Student's t-test was used for (C) and (D) cortex, and Mann–Whitney U-test was performed for (D) hippocampus. In other cases, two-way ANOVA with a *post hoc* Tukey–Kramer test (A, B) or the Student–Newman–Keuls test (E) was used.

Taken together, these data suggest that the pathological modification of BACE1, bisecting GlcNAc, blocks the lysosomal trafficking of BACE1 in the brain.

Increased localization of BACE1 to late endosomes/lysosomes in the absence of GnT-III would enhance its lysosomal degradation and lead to down-regulation of BACE1 protein. Although we could not observe a significant reduction in BACE1 protein in 3-month-old *hAPP/Mgat3*$^{-/-}$ mice (Fig 1C), immunohistochemical (Fig 6A) and Western blot (Fig 6B) analyses demonstrated that the level of BACE1 was significantly lower in 12-month-old *hAPP/Mgat3*$^{-/-}$ animals than in age-matched *hAPP/Mgat3*$^{+/+}$ mice. Similar down-regulation of BACE1 was also observed in *Mgat3*$^{-/-}$ MEFs as compared with *Mgat3*$^{+/+}$ MEFs (Fig 6C), resulting in a significant reduction of Aβ generation in *Mgat3*$^{-/-}$ MEFs (Fig 6D).

Golgi-localized gamma adaptin ear-containing ARF-binding 3 (GGA3) has been reported to promote BACE1 degradation by transporting BACE1 from early endosomes to the late endosome/lysosome pathway (Tesco *et al*, 2007). Knockdown of GGA3 did not affect the level of BACE1 mRNA (Supplementary Fig S4G) but partially rescued the level of BACE1 protein in *Mgat3*$^{-/-}$ MEFs (Fig 6E), suggesting that BACE1 in these cells is indeed abnormally targeted to the late endosome/lysosome pathway in a partially GGA3-dependent manner. These findings indicate that GnT-III deficiency causes BACE1 protein to be relocated from early endosomes (where BACE1 is co-localized with APP) to the late endosome/lysosomal pathway partly via GGA3, eventually leading to increased degradation in lysosomes.

Impaired BACE1 activity in the absence of GnT-III is somewhat selective to APP

In addition to APP, BACE1 cleaves several substrate proteins (Hitt *et al*, 2012; Kuhn *et al*, 2012; Vassar *et al*, 2014; Zhou *et al*, 2012), and targeting BACE1 could therefore affect several physiological phenomena via impaired cleavage of these substrates. Indeed,

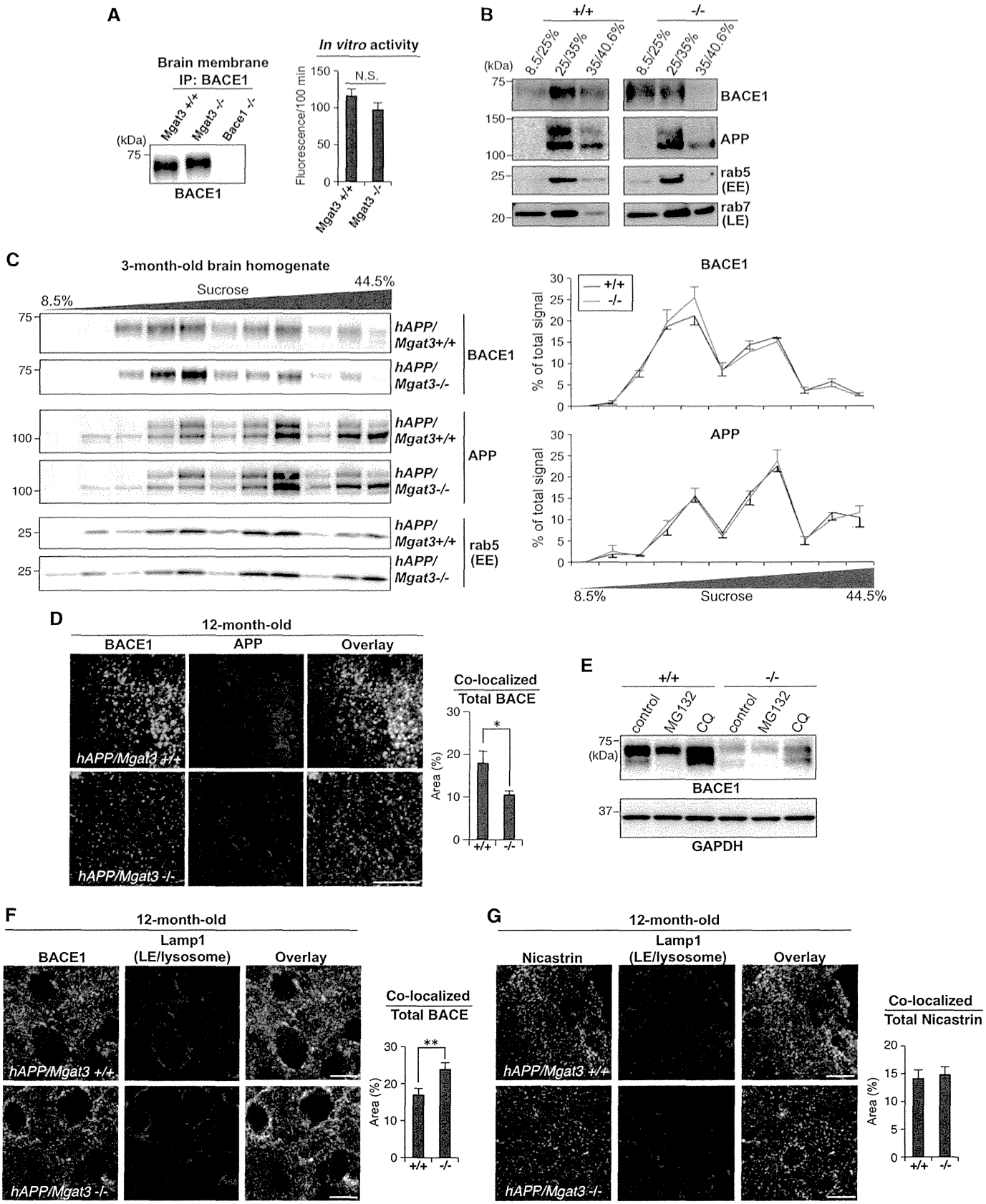

Figure 5.

Figure 5. BACE1 is directed to late endosomes/lysosomes in *Mgat3*$^{-/-}$ cells.

A BACE1 from 2-week-old mouse brains was immunoprecipitated and immunoblotted (left). Immunoprecipitated BACE1 activity was measured *in vitro* (right, n = 3). The values of *Bace1*$^{-/-}$ samples were subtracted as a background. N.S., P = 0.101.

B MEF homogenates were fractionated by sucrose density centrifugation and immunoblotted for BACE1, APP, rab5, or rab7. EE, early endosome; LE, late endosome.

C Brain homogenates were fractionated by sucrose density centrifugation and immunoblotted for BACE1, rab5, or rab9. EE, early endosome; LE, late endosome. Signal intensities were quantified and are shown in the right graphs.

D Immunostaining of 12-month-old mouse cerebral cortex for BACE1 and APP. A typical image in the vicinity of plaque-forming area is shown for *hAPP/Mgat3*$^{+/+}$ brain. The area of co-localization was quantified using random images of cerebral cortex (n = 10). *P = 0.015.

E Immunoblot of BACE1 or GAPDH (loading control) from immortalized MEFs treated with a proteasome inhibitor (MG132) or a lysosome inhibitor (chloroquine; CQ).

F, G Immunostaining of 12-month-old mouse cerebral cortex for BACE1 (F), or nicastrin (G), and Lamp1. LE, late endosome. Scale bar, 10 μm. The area in which co-localized staining was observed was quantified as a percentage of the total BACE1-positive area (right, n = 10). **P = 0.007.

Data information: All graphs show means ± SEM (Student's t-test).
Source data are available online for this figure.

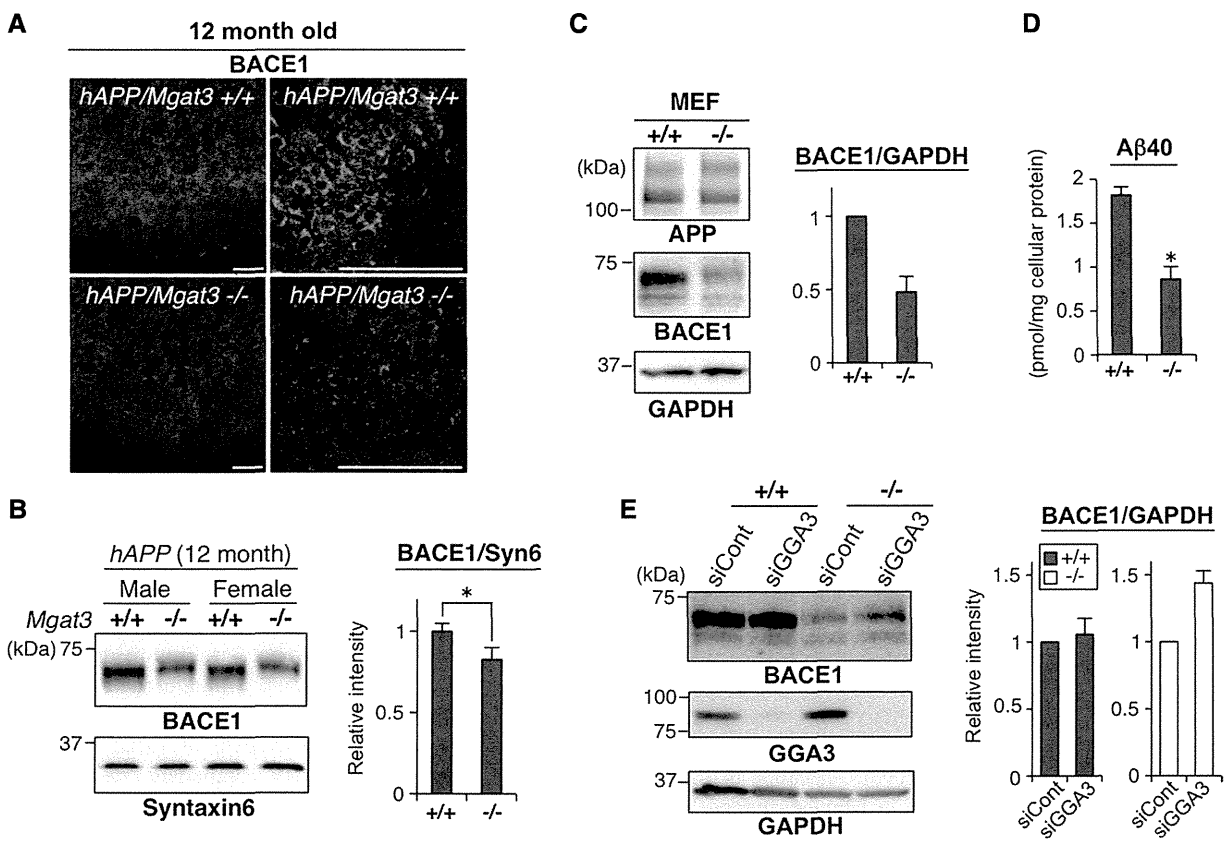

Figure 6. Down-regulation of BACE1 protein in aged *Mgat3*$^{-/-}$ mouse brain.

A Immunostaining of 12-month-old brain sections (cerebral cortex) with anti-BACE1. Scale bar, 100 μm.

B Proteins from the membrane fractions of 12-month-old mouse brains (n = 4–5) were immunoblotted for BACE1, and BACE1 intensity was quantified. *P = 0.044.

C Lysates from MEFs were immunoblotted for APP, BACE1, or GAPDH (loading control), and BACE1 intensity was quantified (n = 4).

D Amount of Aβ40 in the culture medium of immortalized MEFs (n = 3). *P = 0.045.

E MEFs were transfected with control siRNA or GGA3-siRNA and then immunoblotted for BACE1, GGA3, or GAPDH (loading control) (n = 6).

Data Information: All graphs show means ± SEM (*P < 0.05; Student's t-test for (B) and the Mann–Whitney U-test for (D)).
Source data are available online for this figure.

recent studies have reported several abnormalities in *Bace1*$^{-/-}$ mice (Cai *et al*, 2012; Cheret *et al*, 2013; Savonenko *et al*, 2008). Intriguingly, however, the levels of other BACE1 substrates, full-length CHL1, and contactin-2, which were significantly increased in *Bace1*$^{-/-}$ mice due to impaired cleavage, were normal in *Mgat3*$^{-/-}$ mice (Fig 7A). This result indicates that the effect of bisecting GlcNAc on BACE1 is somewhat selective to APP. In addition, although a large number of *Bace1*$^{-/-}$ offspring died within 4 weeks after birth (Fig 7B) (Dominguez *et al*, 2005), *Mgat3*$^{+/-}$ intercrosses produced *Mgat3*$^{-/-}$ mice (23.7%) at normal Mendelian frequency. Moreover, *Mgat3*$^{-/-}$ mice are generally healthy, fertile, and behaviorally normal (Priatel *et al*, 1997). These findings raise the possibility that GnT-III-targeted BACE1 inhibition results in fewer side effects than inhibiting BACE1 itself.

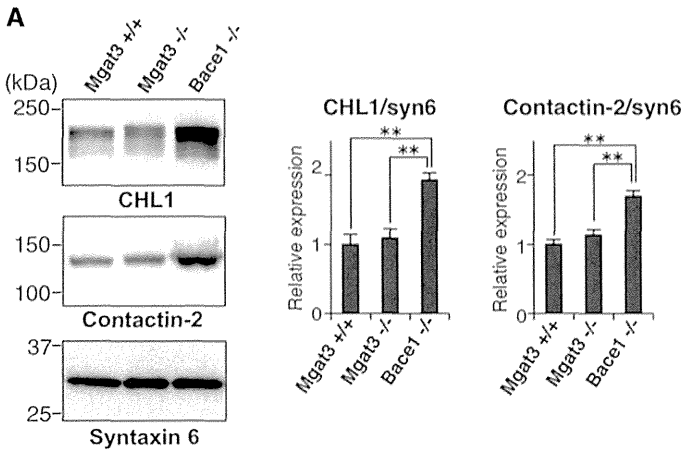

B

Number of pups (at 4-weeks of age) from heterozygous crosses

	+/+	+/-	-/-
Bace1 (*n* = 101)	29 (28.7%)	62 (61.4%)	10 (9.9%)
Mgat3 (*n* = 321)	78 (24.3%)	167 (52.0%)	76 (23.7%)

Figure 7. Limited impairment of BACE1 activity in *Mgat3*$^{-/-}$ brain.

A Membrane fractions from 3-week-old *Mgat3*$^{+/+}$, *Mgat3*$^{-/-}$, and *Bace1*$^{-/-}$ mice were immunoblotted for CHL1 (upper), contactin-2 (middle), or syntaxin 6 (lower) (n = 4–5). The graphs show means ± SEM (**P < 0.01; two-way ANOVA with *post hoc* Tukey–Kramer test, P = 0.006 for *Mgat3*$^{+/+}$ versus *Bace1*$^{-/-}$, P = 0.008 for *Mgat3*$^{-/-}$ versus *Bace1*$^{-/-}$ in CHL1/syn6, P = 0.001 for *Mgat3*$^{+/+}$ versus *Bace1*$^{-/-}$, P = 0.002 for *Mgat3*$^{-/-}$ versus *Bace1*$^{-/-}$ in Contactin-2/syn6).

B Number of pups surviving at 4 weeks following a cross between heterozygous male and female mice.

Source data are available online for this figure.

Discussion

In this study, we first show that BACE1 is highly modified with bisecting GlcNAc in the brains of AD patients. Our analyses of GnT-III-deficient mice show that lack of bisecting GlcNAc causes a shift in the intracellular localization of BACE1 from early endosomes, where the substrate APP is mainly localized, to late endosomes/lysosomes, thereby enhancing its lysosomal degradation. Both events could contribute to the ameliorated AD-related pathology observed in GnT-III-deficient mice via a significant reduction in Aβ generation (Fig 8).

The present study revealed that APP is either not modified or barely modified in the brain (Supplementary Fig S1F), whereas we previously found that it is modified with bisecting GlcNAc in neuroblastoma cells (Akasaka-Manya *et al*, 2008), indicating that bisecting GlcNAc modification on APP occurs in a limited number of cell types. How brain glycoproteins undergo specific glycosylation is another interesting issue.

In addition to Aβ generation, the physiological roles of BACE1 should also be highlighted, given that the use of BACE1 inhibitors as AD therapeutics could disturb these functions. Abnormal phenotypes have been reported in BACE1-deficient mice, including a schizophrenia-like phenotype (Savonenko *et al*, 2008), abnormal muscle spindle formation (Cheret *et al*, 2013), and retinal pathology (Cai *et al*, 2012). Moreover, recent proteomic studies have identified an increased number of novel BACE1 substrates (Kuhn *et al*, 2012; Zhou *et al*, 2012), the biological consequences of whose proteolytic cleavage by BACE1 have not yet been clarified. Unlike BACE1-deficient mice, GnT-III-deficient mice do not display significant abnormalities (Orr *et al*, 2013; Priatel *et al*, 1997), exhibiting only a slight increase in B-220-positive cells and lower vertical activity (Orr *et al*, 2013). Although mutant mice expressing truncated GnT-III have been reported to exhibit several neurological defects such as impaired leg clasp reflex, these abnormalities are considerably milder than those observed in *Bace1*$^{-/-}$ mice and are not seen in GnT-III-deficient mice (Bhattacharyya *et al*, 2002), suggesting that they derive from the presence of truncated GnT-III and not from the loss of full-length GnT-III. These results suggest that inhibiting GnT-III activity would have fewer side effects than the administration of BACE1 inhibitors. Taken together, our findings shed light on the advantages of considering the development of glycan-targeted drugs for AD treatment.

Recent reports have shown that BACE1 is recycled between the Golgi network, the plasma membrane, and endosomes (Tan & Evin, 2012) and that endosomal localization of BACE1 is regulated by GGAs and the retromer, a multiprotein complex required for the recycling of transmembrane proteins from endosomes to the trans-Golgi network. Knockdown of vacuolar protein sorting (Vps) 35, a retromer complex component, results in increased BACE1 localization in endosomes, and *Vps35*$^{+/-}$ mice display increased Aβ generation and deposition (Wen *et al*, 2011). In contrast, the exit of BACE1 from endosomes toward lysosomes is mediated by GGAs, particularly GGA3, which is supported by the finding that *Gga3*$^{-/-}$ brains show increased levels of BACE1 protein (Walker *et al*, 2012). Knockdown of GGA3 partially rescued the instability of BACE1 in *Mgat3*$^{-/-}$ cells, indicating that the absence of bisecting GlcNAc directs BACE1 to the GGA3-mediated lysosomal pathway. It seems that the physical interaction of BACE1 with GGA3 involves the cytoplasmic region of BACE1 and is regulated by BACE1 ubiquitination at the C-terminus (Kang *et al*, 2010), whereas bisected glycans on BACE1 are located in its luminal region, suggesting that an unidentified molecule recognizes bisecting GlcNAc on BACE1 and mediates the interaction between BACE1 and GGA3. We are currently attempting to identify an endogenous lectin-like molecule that displays these properties.

It has been shown that BACE1 is a stress-responsive protease (Kao *et al*, 2004; Vassar *et al*, 2014), and increased BACE1 activity

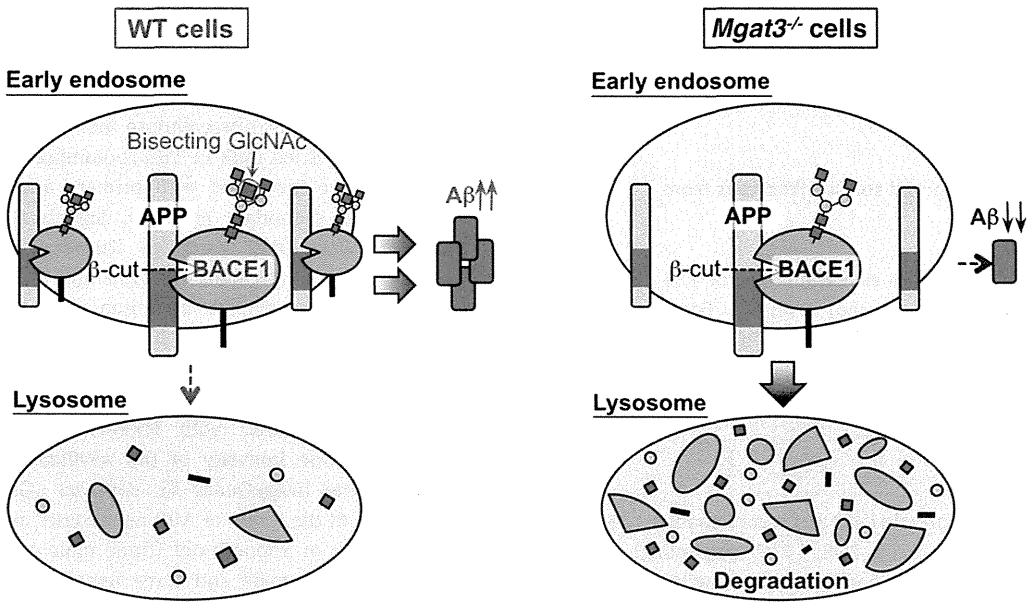

Figure 8. Schematic model of results.
Lack of bisecting GlcNAc relocates BACE1 from early endosomes (Aβ generation site) to lysosomes, leading to a reduction in both Aβ generation and the level of BACE1 protein.

has been observed in AD patients (Yang *et al*, 2003). Our findings demonstrate that BACE1 is highly modified with bisecting GlcNAc in AD patients. Given that bisecting GlcNAc modification is protective for lysosomal degradation of BACE1, we believe that stabilization of BACE1 by this glycan modification also results in enhanced Aβ production in AD patients. Moreover, our finding that BACE1 protein is down-regulated in aged *Mgat3*$^{-/-}$ mice suggests that the regulation of BACE1 by bisecting GlcNAc modification is enhanced with age. Although several studies have previously reported that Aβ-induced stress enhances GnT-III expression in immune cells from AD patients (Fiala *et al*, 2007, 2011), understanding how neuronal GnT-III expression is regulated by oxidative damage or other forms of stress during AD progression remains a topic for future investigation.

Materials and Methods

Antibodies and lectin

The commercially available antibodies used were as follows: rabbit anti-BACE1 (5606), anti-nicastrin (9447S), anti-GGA3 (8027), anti-rab5 (3547), anti-rab7 (9367), and anti-rab9 (5118) from Cell Signaling Technology; anti-APP C-term (recognizes C-terminal part of APP, 18961), anti-APP N-term (10D1), and anti-sAPPβ-sw (10321, clone 6A1) from Immuno-Biological Laboratories; anti-Aβ (SIG-39220, clone 4G8) and anti-sAPPα (SIG-39320, clone 6E10) from SIGNET; anti-Lamp1 (ab25630) and anti-PSD95 (ab2723) from Abcam; anti-actin (A4700) from Sigma; anti-syntaxin 6 (610635) from BD Biosciences; anti-GAPDH (MAB374), anti-APP (22C11), and anti-MBP (MAB386) from Millipore; anti-MAP2 (sc-20172) from Santa Cruz Biotechnology; anti-GFAP (13-0300) from Life Technologies; anti-CHL1 (AF2147) and anti-contactin-2 (AF4439) from R&D systems; and anti-Iba1 (019-197419) from Wako. Biotinylated erythroagglutinating phytohemagglutinin (E4-PHA) lectin was from Seikagaku Corporation.

Mutant mice

The generation of the *Mgat3*-deficient mice, *Bace1*-deficient mice, and transgenic mice expressing human APP with the Swedish mutation (APP23) has been described previously (Luo *et al*, 2001; Priatel *et al*, 1997; Sturchler-Pierrat *et al*, 1997). All mice were from a C57BL/6 genetic background. *Mgat3*-deficient mice were generously provided by Dr. Jamey D. Marth (University of California-Santa Barbara). Mice were housed (3 or fewer mice per cage) at 23 ± 3°C and 55 ± 10% humidity. The light conditions were 14 h : 10 h (lights on at 7:00). All animal experiments were approved by the Animal Experiment Committee of RIKEN.

Staining of Aβ plaques

For immunostaining, 12-month-old mouse brains (three mice per genotype) were fixed with 4% paraformaldehyde in PBS and embedded in paraffin. Paraffin-embedded coronal sections (5 μm thick) were de-paraffinized according to a standard method and then dipped in 90% formic acid for 5 min. After washing with water (5 min), 0.3% H_2O_2 in methanol (30 min), water (10 min), and PBS (3 min), the sections were blocked with 3% BSA in PBS for 30 min, followed by overnight incubation with the primary antibody (1:200 dilution; 4G8). The sections were then incubated with biotinylated anti-mouse IgG, followed by HRP-avidin using the VECTASTAIN ABC standard kit (Vector Laboratories). Signals were visualized by DAB staining. For quantification of the number of Aβ plaques, frozen sections (30 μm thick) from 12-month-old male mice (six mice per genotype) were incubated with 0.05%

(w/v) FSB (Dojindo) in EtOH/PBS (1/1, v/v) for 30 min at room temperature and then washed three times with EtOH/PBS (1/1). Fluorescence was visualized using an Olympus FV-1000 confocal microscope.

Preparation of membrane and soluble fractions from mouse brain

Brains were homogenized with seven volumes of TBS containing a protease inhibitor cocktail (Roche) using a Potter-style tissue grinder. Homogenates were ultracentrifuged at 100,000 × *g* for 30 min at 4°C, and the resultant pellet and supernatant were used as the membrane and soluble fractions, respectively.

Glycosidase treatment

For PNGase F treatment, proteins (50 μg) were denatured by boiling in 20 μl of PBS containing 0.5% SDS, 1% 2-mercaptoethanol, and 4 mM EDTA. After the solution had been diluted with four volumes of PBS containing Nonidet P-40 (NP-40, final concentration 0.5%), PNGase F (1,000 units, New England Biolabs) was added, and the solution was incubated for 3 h at 37°C. For sialidase and *O*-glycosidase treatment, APP was first immunoprecipitated from mouse brain membrane fraction. After washing the beads with TBS/0.1% NP-40, immobilized APP was incubated with 10 mU sialidase (*Arthrobacter ureafaciens*, Nacalai tesque) with or without 1.5 mU *O*-glycosidase (Roche) in acetate buffer (100 mM sodium acetate pH 4.5, 50 mM NaCl, 0.1% NP-40, 1 mM EDTA, protease inhibitor cocktail) for 12 h at 37°C.

Lectin pulldown and immunoprecipitation

For lectin pulldown, the membrane fraction (obtained from 250 μl of homogenate) was solubilized with 750 μl of TBS containing 1% Triton X-100 and a protease inhibitor cocktail (Roche) and then ultracentrifuged at 100,000 × *g* for 15 min. The supernatant was incubated with 100 μl of E4-PHA-agarose (Seikagaku Corporation) for 2 h at 4°C. The beads were washed twice with an excess volume of TBS containing 0.1% Triton X-100, and the bound proteins were eluted with SDS sample buffer. For immunoprecipitation, the membrane fraction (obtained from 250 μl of homogenate) or cell pellet (obtained from a 10-cm dish) was lysed with TBS (750 μl for the brain membrane fraction and 500 μl for the cell pellet) containing 0.5% NP-40 and protease inhibitor cocktails and then ultracentrifuged at 100,000 × *g* for 15 min. The supernatant was incubated with antibody (3–5 μg) for 10 min at 4°C, after which protein G-Sepharose 4 Fast Flow (20 μl, GE Healthcare) was added to the mixture, followed by rotation for 2 h at 4°C. The beads were washed three times with TBS containing 0.1% NP-40, and bound proteins were eluted with SDS sample buffer.

Y-maze test

The Y-maze test was performed using 12-month-old male mice as described previously with minor modifications (Saito *et al*, 2011). Tests were performed at a light intensity of 90 lx at the level of the platform.

Western and lectin blotting

Proteins were separated by 4–20% gradient SDS–PAGE and then transferred to PVDF or nitrocellulose membranes. After incubation with 5% non-fat dried milk in TBS containing 0.1% Tween-20, the membranes were incubated with primary antibody, followed by HRP-conjugated secondary antibody. Signals were detected with SuperSignal West Dura Extended Duration Substrate (Thermo Scientific) using ImageQuant LAS-4000mini (GE Healthcare). For lectin blotting, nitrocellulose membranes were blocked with TBS containing 0.1% Tween-20 for 30 min at room temperature. The membranes were then incubated with biotinylated E4-PHA lectin (1:500) that had been diluted with TBS containing 0.1% Tween-20, followed by incubation with HRP-avidin (VECTASTAIN ABC Standard Kit). The intensity of the resultant protein bands was quantified using ImageQuant TL software (GE Healthcare). For quantification of the levels of APP metabolites and BACE1, proteins from the brains of 3-month-old (three male and two female) and 12-month-old (two male and three female) mice were analyzed. Each set of experiments was repeated at least three times to confirm the results.

Aβ ELISA

Aβ ELISA was performed as described previously (Iwata *et al*, 2004; Saito *et al*, 2011) with slight modifications. Brains from 3-month-old (three male and two female) and 12-month-old (two male and three female) *hAPP* mice or from 3- to 4-month-old (six male and two female) non-*hAPP* mice were homogenized with seven volumes of TBS containing a protease inhibitor cocktail (Roche) using a Potter-style tissue grinder. Homogenates were ultracentrifuged at 100,000 × *g* for 30 min at 4°C, and the resultant supernatant was used as a TBS-soluble fractions. The pellet was then homogenized again in TBS and ultracentrifuged at 100,000 × *g* for 10 min at 4°C. The resultant pellet containing insoluble and membrane-associated Aβ was suspended in 10 volumes of buffer (50 mM Tris–HCl, 6 M guanidine, protease inhibitor cocktail, pH 7.6) and sonicated. After incubation for 1 h at room temperature, a Gu-HCl-extracted fraction was obtained by ultracentrifugation at 100,000 × *g* for 20 min at 25°C. For ELISA, the Gu-HCl fraction was diluted 12-fold with phosphate buffer, and a 1/11 volume of 6M Gu-HCl was added to the soluble fraction to normalize the effect of Gu-HCl. ELISA was carried out using the Human/Rat βamyloid (40) ELISA kit and Human/Rat βamyloid (42) ELISA kit High-Sensitive (Wako). The values in *Bace1*$^{-/-}$ mice were subtracted as a background. In the case of MEFs, cells were cultured with complete culture medium (DMEM supplemented with 10% fetal bovine serum [FBS]) for 24 h, after which the culture medium was collected. Following centrifugation at 10,000 × *g*, the supernatants were directly analyzed by ELISA without dilution. Cells were also collected for protein measurements.

Glycan analysis of BACE1 from mouse brain

One hundred brains from 1-week-old mice were homogenized in 200 ml of buffer (TBS containing a protease inhibitor cocktail) and then centrifuged at 500 × *g* for 10 min to remove the nuclei of the cells. The supernatant was centrifuged at 105,000 × *g* for 2 h, after

which the pellet was lysed with buffer (TBS containing 0.5% NP-40 and a protease inhibitor cocktail), followed by centrifugation at 105,000 × *g* for 2 h. 15 mg of Dynabeads protein G (Life Technologies) was added, followed by 30 min rotation to remove the IgG in the sample. The beads were then removed, and 240 μg of rabbit anti-BACE1 (5606, Cell Signaling Technology) and 40 mg Dynabeads protein G were added. After 60 h of rotation, the beads were collected and washed three times with an excess volume of TBS containing 0.1% NP-40. They were then further washed with 80 μg of BACE1 C-terminal peptide (CLRQQHDDFADDISLLK, 200 μg/ml in TBS 0.1% NP-40) to remove weakly bound proteins, followed by TBS containing 0.1% NP-40. Proteins bound to the beads were eluted by 800 μl of the buffer (50 mM glycine-HCl, pH 2.5), followed by immediate neutralization by adding 18 μl of 1 M Tris–HCl pH 8.5. The solvent was evaporated by SpeedVac, and the proteins were dissolved and separated by SDS–PAGE. After transfer to PDVF membrane and protein staining with Direct Blue, the band corresponding to BACE1 or the IgG heavy chain was excised. *N*-glycans from these glycoproteins were released and analyzed as described previously (Nakano *et al*, 2011) with some modifications. After release and reduction, *N*-glycans were desialylated by incubating with 2 M acetic acid at 80°C for 2 h. *N*-glycan alditols were separated on a carbon column (5 μm HyperCarb, 1 mm I.D. × 100 mm, Thermo Fisher Scientific) using an Accela HPLC pump (flow rate: 50 μl/min). The eluate was continuously introduced into an ESI source (LTQ Orbitrap XL, Thermo Fisher Scientific). MS spectra were obtained in the negative ion mode using Orbitrap MS (mass range m/z 500 to m/z 2,500), and MS/MS spectra were obtained using Iontrap MS. Monoisotopic masses were assigned with possible monosaccharide compositions using the GlycoMod software tool (mass tolerance for precursor ions is ±0.005 Da).

In vitro BACE1 activity assay

Native BACE1 was extracted from the membrane fraction (obtained from 250 μl of homogenate) of 2-week-old mouse brain tissue with TBS containing 1% Triton X-100 and a protease inhibitor cocktail. After centrifugation at 100,000 × *g*, the supernatant was subjected to overnight immunoprecipitation with 5 μg of anti-BACE1 antibody and 20 μl of protein G-Sepharose. The beads were washed twice with TBS containing 0.2% Triton X-100 and used directly as an enzyme source. For preparation of recombinant BACE1-Fc, COS-7 cells were co-transfected with pEF-Fc/BACE1, together with pCXN2, pCXN2/GnT-III, or pCXN2/GnT-III D319A. After 6 h, the medium was replaced with Opti-MEM I followed by further culture for 3 days. Recombinant BACE1 proteins (0.75 μg of each protein), purified through a protein G column, were used as an enzyme source. Assays were performed in a solution containing 100 mM sodium acetate buffer at pH 4.5, 20 μM substrate (3212v, Peptide Institute Inc.), 0.25% Triton X-100, protease inhibitor cocktails, and an enzyme source in a final volume of 50 μl, followed by incubation for 100 min at 37°C. We confirmed that for an incubation period up to 120 min, BACE1 hydrolyzes the substrate in a time- and dose-dependent manner. The reaction was stopped by adding 50 μl of denaturing buffer (1% SDS, 100 mM Tris–HCl pH 9.5), and fluorescence was measured using a Wallac 1420 ARVOsx multilabel counter (Perkin Elmer) at excitation and emission wavelengths of 340 nm and 405 nm, respectively.

Plasmids

The construction of pEF-Fc/human BACE1 (soluble BACE1-Fc) has been described previously (Kitazume *et al*, 2001). pCXN2/human GnT-III was constructed as described previously (Kitada *et al*, 2001). pCXN2/human GnT-III D319A (dominant negative form (Ihara *et al*, 2002)) was constructed using a QuickChange XL Site-Directed Mutagenesis Kit (Agilent Technologies) with primers (GTCTTCATCATTGACGATGCGGCCGAGATCCCGGCCCGTGACG and its complementary sequence). pLenti6/human BACE1 was constructed using PCR to amplify the fragment encoding full-length BACE1 with primers (AGGGAATTCGCCACCATGGCCCAAGCCCTG CCCTG and TCCTCACTTCAGCAGGGAGATGT). The fragment was digested with EcoRI and then inserted into pLenti6/V5-GW/LacZ which had been digested with EcoRI and EcoRV. The plasmid encoding SV40 large T antigen was kindly provided by Dr. Jianguo Gu (Tohoku Pharmaceutical University).

Immunofluorescence staining

To prepare frozen brain sections, mice were transcardially perfused with PBS followed by 4% paraformaldehyde in PBS. Brains were sequentially immersed in the same fixative for 16 h and 30% sucrose in PBS for 3 days (with daily renewal of the buffer) at 4°C. Brain sections (30 μm thick) were stained using the floating method. Briefly, sections were incubated with PBS containing 50 μg/ml digitonin and 3% BSA for 20 min at room temperature, followed by incubation with primary antibody or biotinylated lectin (overnight at 4°C) and Alexa-labeled secondary antibody or streptavidin (30 min at room temperature). For double staining of Aβ plaques, sections were first stained with FSB as described above (see 'Staining of Aβ plaques') and then stained with antibodies. Fluorescence was visualized using an Olympus FV-1000 confocal microscope, with data acquisition and quantification of the signals or co-localized area being carried out using FV10-ASW ver.1.7 software (Olympus).

Preparation of mouse embryonic fibroblasts (MEFs)

Male and female *Mgat3*$^{+/-}$ mice were mated to obtain E13 littermate embryos. After the head and liver were removed from each embryo, the remaining tissues were minced. The cells from each embryo were then incubated at 37°C for 30 min in 5 ml of PBS containing 0.05% trypsin, 0.53 mM EDTA, and 0.004% DNase I. After the cells were collected by centrifugation, they were resuspended and incubated twice for 30 min in the same buffer. They were then suspended in complete culture medium (DMEM supplemented with 10% FBS) before being passed through a 100-μm cell strainer. After centrifugation at 270 × *g* for 5 min at 4°C, the cells were resuspended in the culture medium and plated on a 15-cm dish (one dish per embryo). Genotyping of each embryo was carried out using tissue pieces with the primers described elsewhere (Priatel *et al*, 1997). The MEFs were immortalized by transfection with a plasmid encoding SV40 large T antigen, after which the transformed cells were selected with 400 μg/ml Zeocin.

Preparation of primary neurons

Wild-type (or *Mgat3*$^{-/-}$) male and female mice were crossed, and embryos were used at E16–18. Embryonic brains were minced in